Transient deformation in the Asal-Ghoubbet Rift (Djibouti) since the 1978 diking event: Is deformation controlled by magma supply rates?

D. Smittarello, R. Grandin, J-B de Chabalier, C. Doubre, A. Deprez, F. Masson, A. Socquet, I A Saad

AGU PUBLICATIONS

JGR

Journal of Geophysical Research: Solid Earth

RESEARCH ARTICLE
10.1002/2016JB013069

Key Points:
- Model of the November 1978 rifting event and subsequent postdiking deformation in the Asal Rift
- A central midsegment reservoir feeds a bilateral dike intrusion in 1978
- Magma supply from the central reservoir explains transient postdiking deformation

Supporting Information:
- Supporting Information S1

Correspondence to:
D. Smittarello,
delphine.smittarello@ens.fr

Citation:
Smittarello, D., R. Grandin, J.-B. De Chabalier, C. Doubre, A. Deprez, F. Masson, A. Socquet, and I. A. Saad (2016), Transient deformation in the Asal-Ghoubbet Rift (Djibouti) since the 1978 diking event: Is deformation controlled by magma supply rates?, *J. Geophys. Res. Solid Earth*, *121*, 6030–6052, doi:10.1002/2016JB013069.

Received 8 APR 2016
Accepted 8 JUL 2016
Accepted article online 13 JUL 2016
Published online 1 AUG 2016

Transient deformation in the Asal-Ghoubbet Rift (Djibouti) since the 1978 diking event: Is deformation controlled by magma supply rates?

D. Smittarello[1,2], R. Grandin[1], J.-B. De Chabalier[1], C. Doubre[3], A. Deprez[3,4], F. Masson[3], A. Socquet[4], and I. A. Saad[5]

[1]Institut de Physique du Globe de Paris, Sorbonne Paris Cité, Université Paris Diderot, UMR 7154 CNRS, Paris, France, [2]Département de Géosciences, École Normale Superieure, Paris, France, [3]IPGS/EOST, Université de Strasbourg/CNRS, Strasbourg, France, [4]University Grenoble Alpes, CNRS, ISTerre, Grenoble, France, [5]Observatoire Géophysique d'Arta, Centre d'Etude et de Recherche de Djibouti, Djibouti, Djibouti

Abstract The Asal-Ghoubbet Rift (AG Rift) in Djibouti lies in the subaerial continuation of the Aden ridge system, thereby constituting a unique location to study rifting processes and mechanisms involved in continental breakup and oceanic spreading. Continually upgraded and expanded geodetic technology has been used to record the 1978 Asal rifting event and postdiking deformation. In light of recent results obtained for the Manda Hararo-Dabbahu rifting event (2005–2010), we propose that the horizontal and vertical geodetic data can be modeled with a double source, involving a dike-like inflation component aligned along the rift axis and a spherical pressure source located at midsegment below the Fieale caldera. By revisiting the codiking data, we propose that the reservoir below Fieale could have fed, at least partially, the 1978 injection and the contemporaneous Ardoukôba eruption and potentially induced local subsidence due to magma draining out of the central reservoir. As an alternative to previously proposed viscoelastic relaxation models, we reinterpret postdiking observations using a purely elastic rheology. We determine the relative contribution of a midsegment reservoir inflation and a dike-like opening component, together with their respective time evolutions. Our results suggest that interactions between steadily accumulating tectonic strain and temporal variations in melt supply to the shallow magma plumbing system below the AG Rift may entirely explain the geodetic observations and that viscoelastic deformation processes played a minor role in the 30 years following the 1978 rifting event.

1. Introduction

Extension at the boundary between tectonic plates involves magmatic and tectonic processes that lead from continental breakup to oceanic spreading [*Ebinger and Casey*, 2001]. As breakup proceeds, spreading by magma injection becomes predominant over brittle failure accommodated by tectonic faulting. Injection of magma into dikes tends to localize in narrow, hot, and weak zones during rifting episodes, which are characterized by an intense magmatic and seismic activity associated with significant (metric) surface displacements. These episodes release stresses previously accumulated in the lithosphere during periods of quiescence that can last several hundred to thousands of years [*Björnsson*, 1985] and the intrusions accommodate a large percentage of plate opening [e.g., *Einarsson*, 1991].

Observations and data collected in eroded rift zones, passive volcanic margins, slow-spreading Mid-Oceanic Ridges (Iceland, Mid-Atlantic Ridge) and incipient spreading centers (East Africa) all concur to suggest that injections of magma into dikes initiate from a central and shallow (<6 km) magma reservoir at the middle of the rift segments and migrate laterally toward segment ends [*Einarsson*, 1991; *Hayward and Ebinger*, 1996; *Ebinger and Casey*, 2001; *Keir et al.*, 2009; *Speight et al.*, 1982; *Callot et al.*, 2001; *Doubre and Geoffroy*, 2003]. The phenomenon of lateral magma injection is generally considered well explained within the framework of hydraulic fracturing theory [*Delaney et al.*, 1986; *Rubin*, 1992; *Fialko and Rubin*, 1998; *Rivalta*, 2010; *Grandin et al.*, 2012]. In contrast, processes governing the evolution of the source reservoir prior to and after injections are poorly understood. It is believed that the periodicity and volume of injections are primarily related to the mechanical resistance of the central reservoir combined with the state of pressure within the reservoir [*Buck et al.*, 2006]. As fault activity seems to be strongly modulated by intrusive activity [*Medynski et al.*, 2016], this central magma plumbing system exerts primary control on the organization of the rift zone.

However, the detailed architecture of the magma plumbing system of rift zones at crustal or mantle levels and its evolution over time remain a major unknown, even along slow-spreading segments, where seafloor geophysical monitoring is difficult to maintain.

The surface deformation field over the years following a dike injection gives crucial clues on the nature of the source reservoir. In addition to the 1978 Asal episode (Afar), most observations of codiking and postdiking deformation originate from the Krafla (Iceland) and Manda Hararo (Afar) rifting episodes. These latter episodes involved several, successive dike injections clustered in a period of approximately 10 years, with a total volume of injected material of the order of 1 km^3. Dikes were fed laterally along volcanic rift segments from a central midsegment reservoir, with only a fraction of the magma being emitted at the surface. In both cases, an enhanced spreading rate was observed across the rifts in the years following the last dike intrusion [*Björnsson*, 1985; *Pagli et al.*, 2014]. Two distinct processes have been proposed to account for this observation: continued dike inflation at depth [*Hofton and Foulger*, 1996; *Grandin et al.*, 2010a] or viscous relaxation below a shallow elastic upper crust [*Foulger et al.*, 1992; *Hofton and Foulger*, 1996; *Heki et al.*, 1993; *Nooner et al.*, 2009; *Hamling et al.*, 2010]. In addition, several studies have provided evidences indicating the important role of a concurrent reinflation of the central magma reservoir in the months/years following the intrusions [*Björnsson*, 1985; *Heki et al.*, 1993; *Grandin et al.*, 2010a; *Hamling et al.*, 2014]. Dense observations in space and time are crucial to draw a clear distinction between these different processes.

In this study, in light of the lessons learned from the Krafla and Manda Hararo rifting episodes, we revisit the deformation data in the Asal-Ghoubbet (AG) Rift over the rifting cycle (codiking, postdiking, and interdiking periods), since this rift experienced a single dike injection in 1978. For this purpose, we use more than 40 years of geodetic data, routinely collected since 1972. Codiking data have already been published whereas the quasi-annual geodetic campaigns carried out between 1979 and 1990 have never been systematically exploited.

Given the lack of a 3-D imaging of the whole AG Rift which would help to correctly select the rheological parameters of the rift structure, we choose a simple linear elastic model to reveal the common temporal evolution captured by the geodetic data set.

We first estimate an interdiking deformation model derived from recent GPS observations. This model is used to cancel the steady state contribution due to plate spreading that affect the whole data set. After applying this correction, we carry out a time series inversion of the postdiking data in order to constrain the evolution of transient sources from the 1978 dike intrusion to the present.

In agreement with *Cattin et al.* [2005], we highlight the relevance of a persistent dike-like opening below the rift inner floor, combined with inflation of a midsegment magma reservoir, to fully explain first-order features of the data set. Furthermore, we explore the role of inflation of a midsegment magma reservoir below the current caldera of the Fieale central volcano in explaining rapid postdiking deformation observed in the decade following the 1978 dike intrusion. Finally, we reinterpret data covering the dike intrusion event of 1978 with an elastic inverse model. We test whether the midsegment reservoir below Fieale could have fed, at least partially, the 1978 dike injection and the contemporaneous Ardoukôba eruption, while inducing local subsidence due to magma draining out of the reservoir.

2. General Background of the 1978 Asal-Ghoubbet Rifting Event

2.1. Geological Context

The Afar triple junction lies between the diverging Arabia, Nubia, and Somalia plates (Figure 1a). It forms a large depression where extension and volcanism during the Quaternary are localized along rift segments considered as forming the inland continuation of the divergent plates boundaries, which however are not directly connected. A series of north-south trending volcano-tectonic segments, including the Manda Hararo rift segment, form the southern continuation of the Red Sea spreading center. The Aden oceanic ridge propagates westward through the Gulf of Tadjoura and inland into eastern Afar along the segments of Asal-Ghoubbet and Manda Inakir (Figure 1).

The Asal-Ghoubbet (AG) Rift is a 30 km long segment lying between the Ghoubbet Pass and Lake Asal. The central part of this segment is above water between the two basins of Lake Asal and Ghoubbet Bay. Its 300–800 m deep rift valley is flanked by two conjugate sets of imbricated normal faults, with subvertical scarps up to 150 m. The rift is narrower in its subaerial part (2–3 km) than toward its ends (8–10 km),

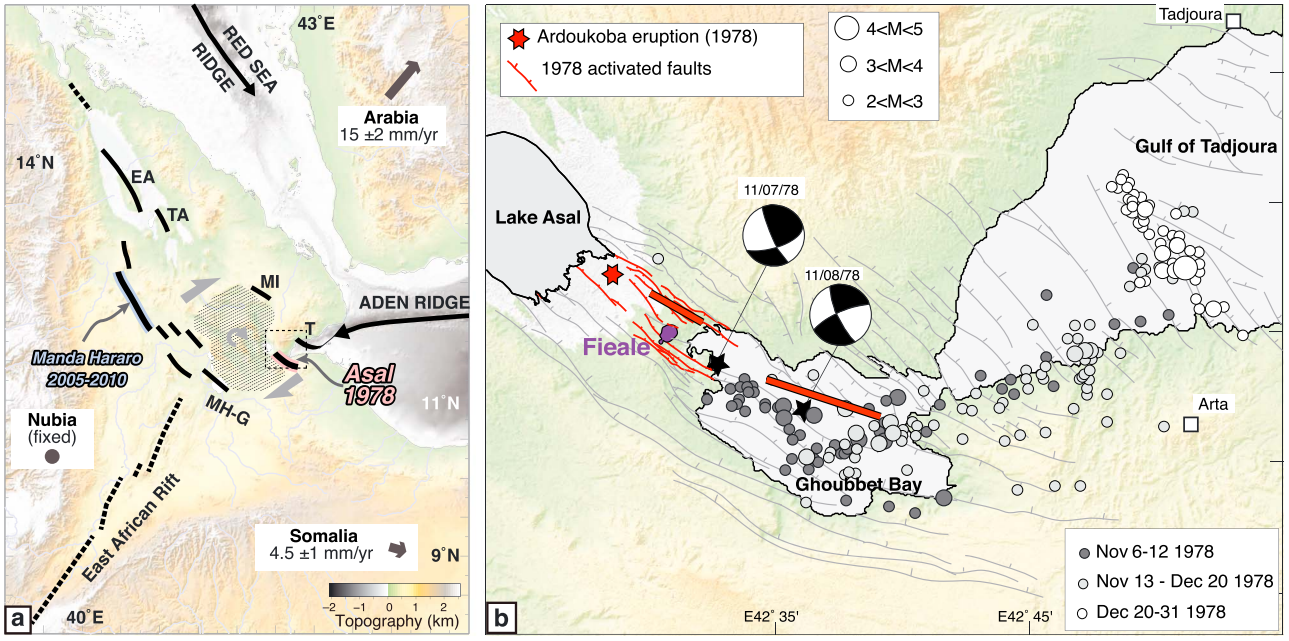

Figure 1. (a) Tectonic map of the Afar depression. Black segments indicate the location of the major rift segments active during the Holocene [from *Manighetti et al.*, 1998; *Hayward and Ebinger*, 1996]. EA: Erta Ale; MH-G: Manda Hararo-Goba'ad; MI: Manda Inakir; T: Tadjoura; TA: Tat'Ali. (b) Seismotectonic map of the 1978 rifting event in the Asal Rift. Seismicity of the first three months (circles) and focal mechanisms come from *Lépine et al.* [1980], major faults (grey lines) from *Manighetti et al.* [1998] and 1978 activated faults (thin red lines) from *Le Dain et al.* [1980]. The dike segments modeled by *Tarantola et al.* [1980] to explain the geodetic data are represented by the two thick red lines. Ardoukôba eruption site is indicated by the red star.

exhibiting the so-called hourglass morphology characteristic of the second-order segmentation of slow-spreading oceanic ridges [*de Vries and Merle*, 1996]. The onset of the opening localization at the AG Rift is dated to 1 Ma [*Manighetti et al.*, 1998]. Recent tectonic-volcanic activity is focused at the rift axis, as attested to by the distribution of fresh basaltic lava flows and the observation of deformed paleoshorelines from the last lake highstand dating of 8–6 ka [*Gasse and Fontes*, 1989; *Stein et al.*, 1991].

The current topography of the subaerial part of the AG Rift has been shown to result from a magmatic phase that built the Fieale central volcano about 100 ka ago, followed by a tectonic phase, i.e., a magma-poor period, during which active normal faults have dismantled the edifice [*De Chabalier and Avouac*, 1994; *Manighetti et al.*, 1998]. This central volcanic system seems to have persisted up to now below the current 1 km diameter caldera located at the center of the segment on its subaerial part, as suggested by the concentrated geothermal activity (fumaroles), the intermittent microseismic activity, the presence of a low seismic velocity anomaly below 3.5 km depth, and the focusing of present-day fault creep activity above the inferred reservoir [*Doubre et al.*, 2007a, 2007b; *Doubre and Peltzer*, 2007].

2.2. The 1978 Event

In November 1978, a seismovolcanic event started in the AG rift, with the occurrence of an intense seismic swarm with two moderate earthquakes of magnitude greater than 5 (maximum magnitude $M_b = 5.3$) and a 1 week long basaltic fissural eruption that led to the extrusion of $10–20 \times 10^6$ m^3 of lava and gave birth to the Ardoukôba volcano (Figure 1b) [*Allard and Tazieff*, 1979]. Tectonic observations and remeasurements of geodetic networks revealed 2 m of extension perpendicular to the rift axis, 70 cm of absolute subsidence of the inner floor accommodated by normal faulting, and 20 cm of absolute uplift of the rift shoulders [*Abdallah et al.*, 1979; *Ruegg et al.*, 1979]. According to an elastic model, these surface displacements have been explained by the injection of two magma-filled dikes below the Ghoubbet Bay and below the subaerial part of the AG Rift, over a length of ~25 km (Figure 1b, in red) [*Tarantola et al.*, 1979, 1980]. Associated with this event, an intense seismic activity of 5 days was recorded (6–10 November 1978) with the epicenters drawing a remarkable N120°E trending alignment within the Ghoubbet Bay (Figure 1b) [*Lépine et al.*, 1980], consistent with a dike injection. After the event, the recorded seismicity continued for 2 months and primarily affected the area of the Ghoubbet Pass and the transfer zone between the AG Rift and the Tadjoura submerged rift segment [*Lépine et al.*, 1980; *Manighetti et al.*, 1998]. At shallow depth, rift extension is accommodated by normal faulting and

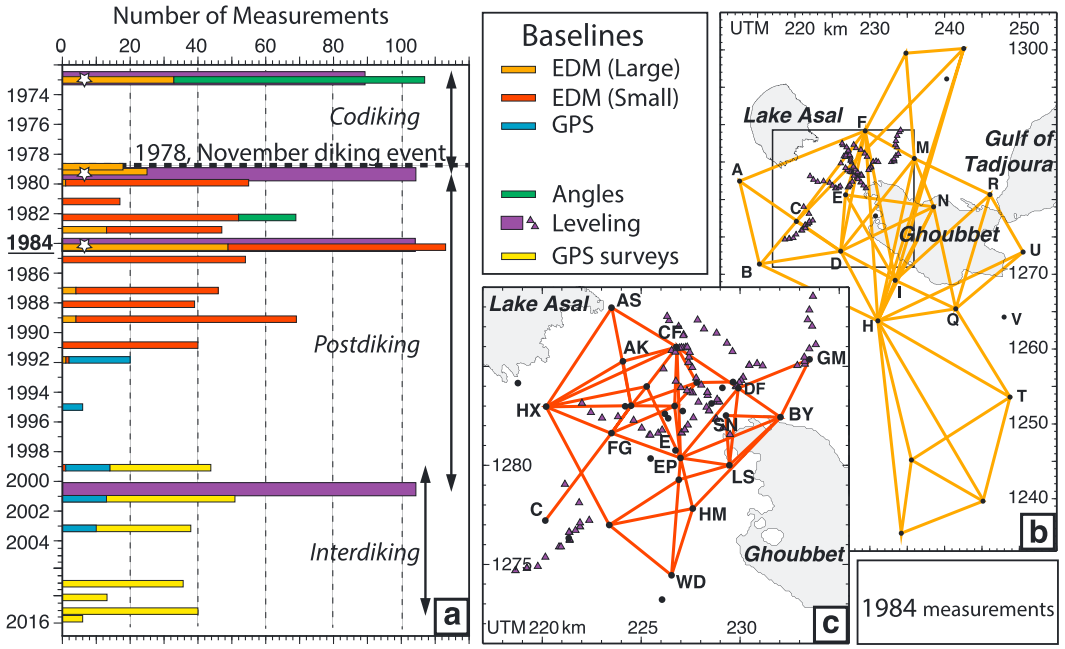

Figure 2. Geodetic data acquired from 1973 to 2014 in the Asal-Ghoubbet Rift. (a) The histogram presents the number of measurements per year as a function of time : number of Electronic Distance Measurements (EDM) for terrestrial geodesy, number of benchmarks measured during GPS surveys and leveling campaigns. White stars locate the three surveys (1973, 1978–1979, and 1984) where data are suitable for network adjustment. An example of survey (for 1984) is represented for (b) the large aperture network ("Large") and for (c) the intrarift network ("Small").

opening fissures within the subaerial part of the rift and the Ghoubbet seafloor [*Le Dain et al.*, 1980; *Audin et al.*, 2001], although the precise geometrical and kinematic relationship between the dike and faults/fissures remains unclear [*Rubin and Pollard*, 1988].

2.3. Post-1978 Deformation

2.3.1. Observations

In order to follow the postrifting deformation, a dedicated "intrarift" geodetic network was established in December 1979 (Figure 2c). A rapid extension, reaching a rate of 5–6 cm yr^{-1} across the rift, was observed in the first decade following the 1978 event [*Ruegg and Kasser*, 1987; *Kasser et al.*, 1987] and then slowed down to 1.5–2 cm yr^{-1} around 1986 (Figure 3b).

Remeasurements of the leveling profile crossing the AG Rift in 1984 and 2000 showed the continuation of a relative subsidence of the rift axis with respect to the rift shoulders accompagnied by localized faulting at shallow depth. This local subsidence is superimposed onto a larger-scale uplift signal of the whole AG rift segment (Figure 4). The seismic activity between 1979 and 1984 was characterized by moderate earthquakes ($M > 2.0$), mainly concentrated below the subaerial part of the rift and located northeast of the rift axis [*Doubre et al.*, 2007b].

A slow down of the vertical deformation rate also occurred some time after 1984 (Figure 4), as the seismicity mainly concentrated near the Fieale caldera.

Since the 1990s, Global Positioning System (GPS) and DORIS measurements [*Souriau et al.*, 1991] have shown that extension across the AG Rift has stabilized to 1.6 cm yr^{-1} [*Vigny et al.*, 2007]. This extension rate is close to the far-field relative velocity of Arabia with respect to Somalia measured by large-scale geodesy [*Jestin et al.*, 1994; *Vigny et al.*, 2006]. This rate is also consistent with the long-term opening velocity of the AG Rift [*De Chabalier and Avouac*, 1994; *Manighetti et al.*, 1998]. This suggests that the transient and rapid deformation from the postdiking phase has lasted ~10 years. Today, despite small fluctuations of seismic activity [*Doubre et al.*, 2007a, 2007b] and minor transient slip events on fissures and faults observed by interferometric synthetic aperture radar (InSAR) [*Doubre and Peltzer*, 2007], a steady state regime, hereafter called "the interdiking phase," appears to have been reached.

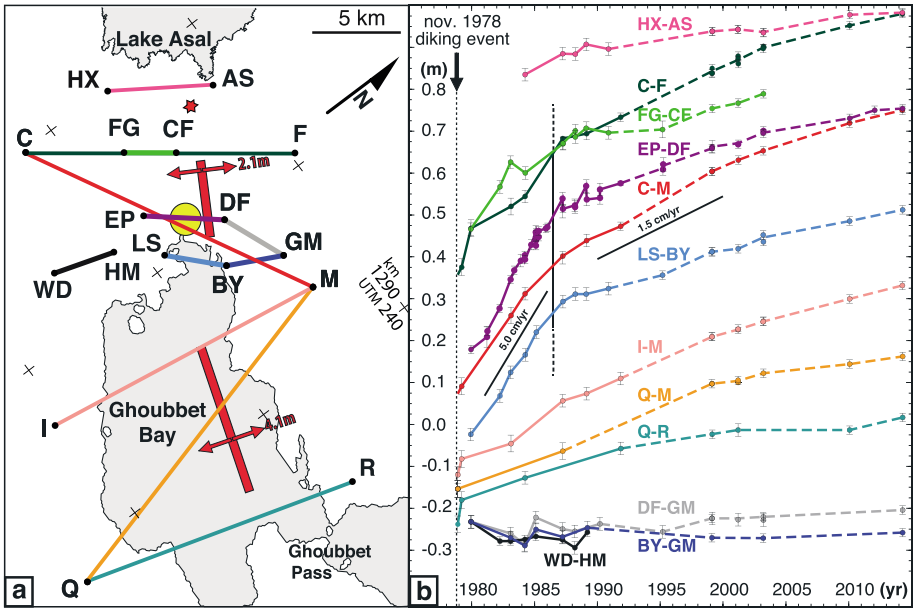

Figure 3. (a) Location of selected benchmarks and baselines across the Asal-Ghoubbet (AG) Rift. The thick red lines represent the dikes with their amount of opening modeled by *Tarantola et al.* [1980]. Red star locates Ardoukôba volcano; yellow circle indicates Fieale caldera. (b) Temporal variation of the selected baselines across the AG Rift after the November 1978 rifting event (same color as in Figure 3a). Continuous lines correspond to EDM measurements whereas dashed lines represent baselines derived from GPS observations. From top to bottom, baselines crossing the rift axis are plotted from NW (Lake Asal) to SE (Ghoubbet Bay), except for the last three baselines which are located on the rift shoulders in the center of the segment.

2.3.2. Previous Interpretations

No consensus has been found regarding the actual processes explaining the postdiking observations in the AG Rift. Using the geodetic data from 1979 to 1984, *Bekoa* [1986] proposed that deformation was induced by inflation of a magma chamber modeled as a horizontal cylindric pressure source lying at 4 km depth and parallel to the rift axis. *Cattin et al.* [2005] designed a two-dimensional thermomechanical model to determine the dominant process governing postrifting deformation in the same period. They explained the enhanced opening rate observed after the 1978 dike injection by a persistent dike opening rate of 12 cm yr^{-1} ending abruptly in 1985, dismissing viscous relaxation as a dominant process. They also argued that magma chamber inflation played a minor role during the early postdiking period. *Vigny et al.* [2007] attempted to account for the temporal evolution of baselines across the rift between 1979 and 1989 using a viscoelastic stress diffusion model. They interpreted the temporal evolution of deformation as continuous in time, arguing that the velocity change observed between 1980 and 2003 is progressive.

While the latter mechanism (viscoelastic relaxation) is in line with models previously proposed to account for transient displacements observed in the years/decades following large tectonic earthquakes, the former mechanisms (intrusion/inflation) put the emphasis on the role of magmatic processes.

The apparent inconsistencies among the above studies likely reflect the use of distinct parts of the data set: either (1) a selected set of baselines was used, reducing the complexity of the information, or (2) displacement vectors derived from an unstable network adjustment were used (see details in section S2 of the supporting information), resulting in a problematic fit with the observations. Furthermore, modeling was carried out in two dimensions, thereby discarding the role of rift-parallel displacements. Yet this component contains crucial information on the shape and along-axis dimension of inferred sources of deformation. The only exception is the work of *Cattin et al.* [2005], who tested a Mogi inflation model against observed displacement vectors and leveling data. Unfortunately, their Mogi source was located in the vicinity of the Ardoukôba fissure eruption, leading the authors to dismiss this scenario due to a poor fit with the observations. In the following, we will show that moving the pressure source to the location of the Fieale central magma reservoir, as suggested by the geophysical and field observations presented above, leads to improved agreement with geodetic observations.

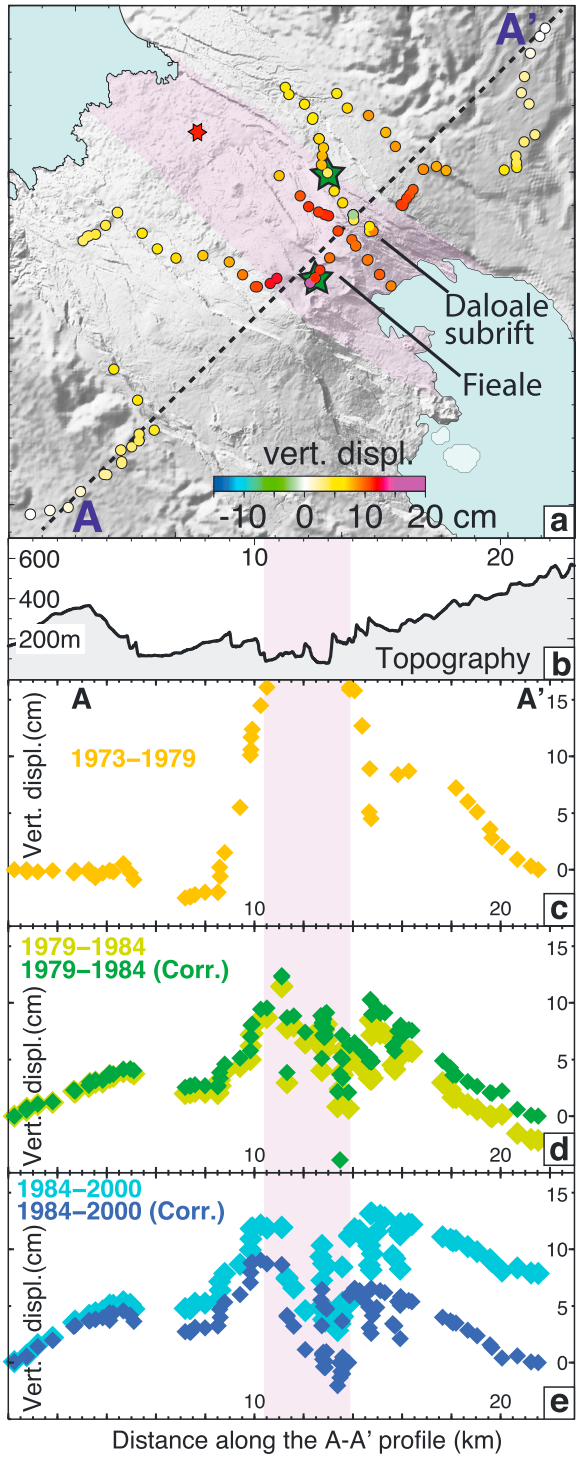

Figure 4. Leveling data. (a) Map view of the leveling benchmarks represented by the circles colored as a function of vertical displacements between 1979 and 1984. The purple-shaded area locates the inner floor, where subsidence relative to the rift shoulders is controlled by faulting. Leveling measurements in this area are excluded from the modeling. The green stars locate the microleveling areas of Fieale and Daloale, where vertical throws have been measured over time and the red star Ardoukoba volcano. (b) Topographic cross section of the rift, along the A-A' profile indicated in Figure 4a by the black dotted line. (c) Vertical displacements over the 1973–1979 interval. (d) Vertical displacements over the 1979–1984 interval with measurements (in light green) and corrected (in green). (e) Vertical displacements over the 1984–2000 interval with measurements (in light blue) and corrected (in blue). See text and supporting information for details.

3. Data

Due to its morphology and location, the AG rift segment (Figure 1b) has been recognized since the 1960s as a privileged target to study rifting processes and mechanisms involved in continental breakup and oceanic spreading [*Tazieff and Varet*, 1972].

The Arta Geophysical Observatory was created in 1972 with the deployment of seismic stations throughout the former *Territoire français des Afar et des Issas*. The geodetic measurements carried out in the AG Rift have followed the evolution of the technological developments, leading to great heterogeneity within this large data set (Figure 2a) (e.g., see *Dzurisin* [2007], for a review of the successive geodetic techniques developed in the second half of the 20th century). Appropriate processing and analysis strategies are therefore required to thoroughly contend with the heterogeneity of the data set.

3.1. Precise Leveling Line

In the winter of 1972–1973 a precise leveling line was established along a 60 km long track crossing the AG Rift, meandering from the shoulders to the inner floor of the rift (Figures 2b, 2c, and 4a). The line was resurveyed in March 1979, 1984, and 2000, allowing to derive vertical displacement in three time intervals [*IGN et al.*, 1973].

The 1978 dike intrusion is captured by the first interval (1973–1979), whereas the two subsequent intervals span the postdiking phase (1979–1984 and 1984–2000). The 1972–1973 and 1978–1979 surveys were conducted in double runs, whereas the 1984 and 2000 surveys were single runs, leading to larger errors [*Ruegg and Kasser*, 1987; *Ballu et al.*, 2003]. This likely explains the observed assymmetry of the leveling profiles in the two postdiking intervals (Figure 4). This assymmetry is canceled empirically prior to modeling (see section S1 in the supporting information, for details on the correction). In the following, the corrected vertical displacements will be considered in priority but the uncorrected vertical displacement profiles will be also presented for comparison. The correction has little impact on the modeling results presented thereafter, as the large-scale assymmetry cannot be reproduced by our symmetrical deformation models.

After the main event of 1978, two short leveling lines have been established in the Fieale caldera and in the Daloale subrift (Figure 4, green stars) to survey creep on some active faults within the rift inner floor. Monthly surveys provide evidence of the creeping of these two faults, at a rate of 5 to 10 mm yr^{-1} decreasing over the 8 years following the event [*Kasser et al.*, 1987]. These data are not used in the modeling, but will be considered in the discussion.

3.2. Geodetic Networks

3.2.1. Large Aperture Triangulation-Trilateration Network

During the winter of 1972–1973, geodesists from IGN (France) in collaboration with IPGP (France) established a large triangulation network across the AG Rift and its shoulders (Figure 2b). The triangulation network is composed of 22 points covering an area of 70×50 km^2, yielding a mesh of 10–20 km. The initial survey consisted of azimuth angle measurements with first-order triangulation precision, scaled by distance measurements with AGA8 geodimeter on about one third of the observed sides. Horizontal coordinates with an accuracy of ~2.5 cm have been obtained by classical trilateration-triangulation (i.e., least squares adjustment of the observational errors). After the diking event of November 1978, this network was partially remeasured both in December 1978 and March 1979, using the newly developed laser instrument Rangemaster III and AGA8. Adjusted coordinates deduced from the 1973 and 1978–1979 surveys allow us, by subtraction, to derive vectors associated with the corifting period [*Ruegg et al.*, 1979]. A complete remeasurement of the network was carried out in 1984, and partially in 1983, 1987 and 1989 (Figure 2a). With the improvement of the accuracy of Electromagnetic Distance Measurements (EDM), azimuth angle measurements have been abandoned after 1973 which has led to some difficulties in the adjustment process (see details in section S2).

3.2.2. Intrarift Trilateration Network

In order to follow in detail the postrifting deformation and resolve the contribution of the faults, fissures, and active subregions of the rift, a smaller "intrarift" network was established in December 1979 (Figure 2c). The network consists of ~20 benchmarks (mesh of 3–10 km) exclusively located on the subaerial part of the AG Rift. Trilateration surveys were carried out almost annually with AGA14 and AGA600 geodimeters from 1979 to 1991 (Figure 2a). The most complete surveys (1979 and 1984) can be adjusted to settle coordinates and derive vectors, whereas insufficient redundancy in other surveys makes network adjustment unstable.

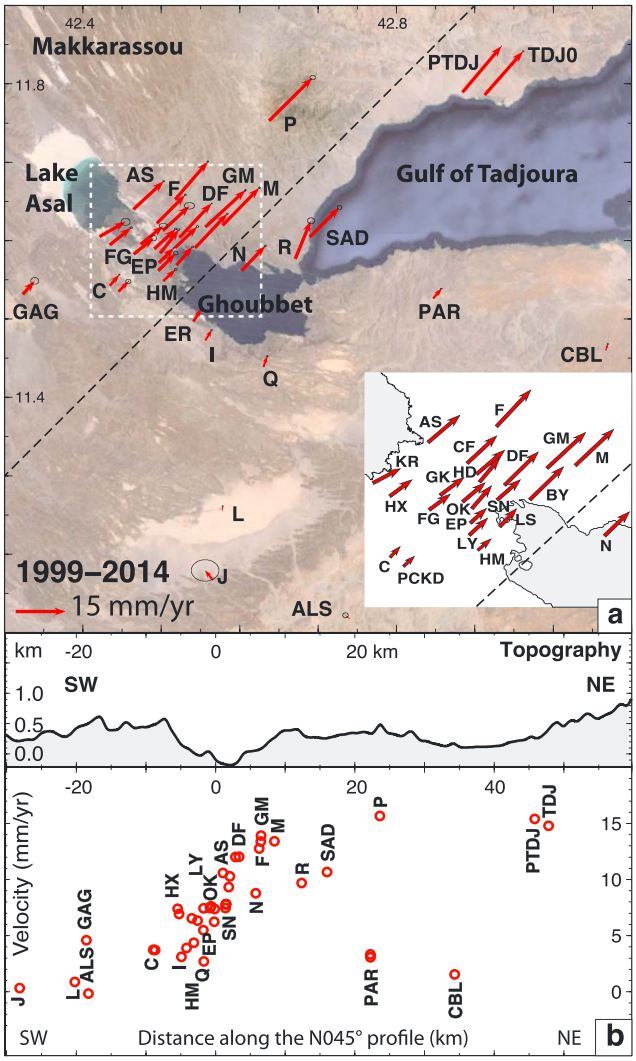

Figure 5. (a) Horizontal velocity field from GPS data in the 1999–2014 interval with inset enlarged for the Asal Ghoubet area (white dotted line). Velocities are referenced with respect to Somalia plate [*Déprez et al.*, 2013, 2015]. The black dotted line locates the N45°E profile of the topographic cross section presented in the center. The same length scale for opening vectors is used in the figure and in the inset. (b) Velocity vectors projected along the N45°E profile.

For this reason, only the 1979–1984/1985 postdiking horizontal displacement field has been published thus far [*Ruegg and Kasser*, 1987]. In contrast, because of the instability of the network adjustment, other annual measurements have never been used to analyze in detail the space-time evolution of the deformation field over the whole postdiking phase.

3.2.3. GPS Surveys

The first GPS measurements in the AG Rift started in 1987. In the 1990s the poor accuracy only allowed for the calculation of baseline variations and therefore only complement the terrestrial geodetic database mainly for the large-scale network. From 1999, with the improvement of the positioning accuracy (increase of the number of satellites, improvement of the orbits), repeated GPS surveys of both the large and small aperture networks provide the first consistent velocity field within the AG Rift and surrounding areas (Figure 5) [*Vigny et al.*, 2007]. The whole network has been comprehensively measured in 2001, 2003, 2010, and 2014, and partly in 2012. Some specific sites are annually measured together with the four to six continuous GPS stations deployed within and around the rift since 2004, which largely improved the accuracy of the velocity field.

4. Modeling Strategy

4.1. Data Analysis

We first break down the entire research period (1973–2014) into three with time limits established from the temporal evolution of the displacements measured across the rift (Figure 3), taking into account the temporal sampling of the measurements (Figures 2a):

1. the codiking period, consisting of the difference between 1973 and 1978–1979 large aperture trilateration network and leveling line data,
2. the postdiking period, integrating all the available baseline and leveling data from December 1978 to 2000 (throughout the text, the term "postdiking" refers to events or observations taking place after the 1978 dike intrusion, with no assumption implied on the actual process at stake, whether magmatic, viscous or brittle in nature), and
3. the interdiking period, using the velocity field determined from GPS measurements between 1999 and 2014. The inception time of the interdiking period is based on the observation that opening rates across the AG Rift appear to have remained stable since 1999 (Figure 3).

Figure 3 presents the temporal evolution of selected baselines plotted from Lake Asal to Ghoubbet Bay from 1978 to 2014. The baselines crossing the center of the segment, i.e., next to Fieale, display significantly larger postdiking extension (C-F to LS-BY, ~30 cm over 10 years), compared to the baselines crossing the Ghoubbet Bay (I-M to Q-R, ~15 cm over 10 years). In contrast, maximum opening during the codiking period in 1978 occurred in the Ghoubbet Bay (baselines increase of 2 m) whereas the opening across the subaerial AG Rift reached 0.6 m, as shown in Figure 3a [*Ruegg et al.*, 1979]). Elastic modeling indicates that the latter measurements are consistent with an opening twice as large in Ghoubbet (4 m of opening compared to 2 m in the subaerial AG Rift [*Tarantola et al.*, 1979]). Furthermore, the time evolution of the baseline lengths for points located across the center of the segment displays an abrupt velocity decrease around 1986, from about 5 cm yr^{-1} to 1.5 cm yr^{-1}. Spatially, this rate change is not observed for the baselines crossing the extremities of the segment, i.e., in Lake Asal and in the Ghoubbet Pass areas, where the opening velocity for the whole postdiking period remains close to the steady state interdiking rate throughout the whole postdiking period (Figure 3a).

Vertical postrifting deformation reveals a large-scale uplift with a maximum of ~15 cm, centered at the rift axis, for the periods 1978–1984 and 1984–2000 (Figure 4c). If one extrapolates a mean velocity for each period, these observations suggest a decrease of the uplift rate with time, with a maximum uplift rate of 2.5 cm yr^{-1} and 1 cm yr^{-1} for early and late postdiking periods, respectively. As shown by the short profiles parallel to rift axis, the maximum of uplift is also symmetrical with respect to the topographic high within the rift inner floor, centered at the Fieale caldera (Figure 4a).

To conclude, since the main locus of deformation during the coperiod and postperiod occurs in distinct locations, the observed postdiking deformation cannot be explained by a simple viscoelastic relaxation model [e.g., *Nooner et al.*, 2009].

Therefore, we propose to test whether most of the postdiking deformation is caused by magmatic processes that take place at the center of the segment. To do so, we reinterpret the postdiking observations according to this assumption, which will be further discussed in section 6.2.

4.2. Inversion Procedure

The strategy used in this work follows a succession of three steps (Figure 6). The deformation field measured across the AG Rift after November 1978 is interpreted as a superposition of (1) a steady state deformation field induced by stretching of the plate boundary over a broad scale and (2) a transient postdiking deformation signal that we seek to model. The velocity field estimated from GPS campaigns and permanent stations from 1999 to 2014 is first used to derive an interdiking model that accounts for the steady state component of deformation across the AG Rift (section 5.1). This model is then used to correct the horizontal (baselines) and vertical (leveling) measurements acquired between 1978 and 2003. Next, to model the postdiking deformation we proceed in three substeps (section 5.2). First, we identify the sources required to explain the data (section 5.2.1) and examine a dike source and a pressure source. We use the 1978–1979 and 1984 data (which correspond to the most complete baseline surveys) to apply an adapted methodology of network adjustment and derive the displacement vectors. These vectors combined with leveling data are used to solve the nonlinear problem of the sources geometry, in particular, their location. Second, we directly use the baseline

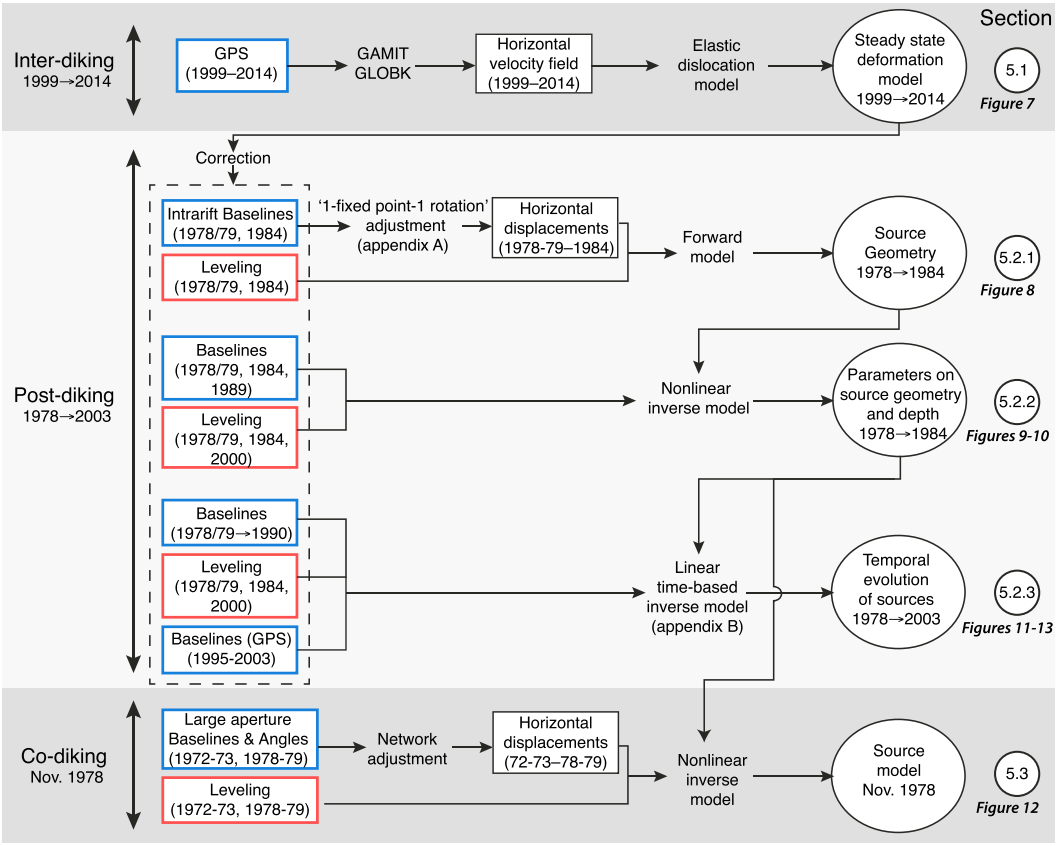

Figure 6. Data sets and modeling strategy.

variations and leveling data acquired in 1978–1979, 1984, and 1989 to improve the geometry of the sources (section 5.2.2). Third, after holding the geometry fixed, we use the complete data set (i.e., all baseline and leveling measurements) to solve the linear problem of the temporal evolution of inflation rates between 1978 and 2003 (section 5.2.3). Finally, the same geometry, extrapolated in the Ghoubbet Bay, is used to carry out an inversion of the 1973 and 1978–1979 data and to revisit the codiking event of November 1978 (section 5.3).

5. Models

5.1. Interdiking Period (1999–2014)

We determine the steady state component of deformation across AG Rift by using GPS measurements from 1999 to 2014 referenced to a fixed Somalia plate (Figure 5a). Those velocity vectors projected along azimuth N045°E (Figure 5b) show a large-scale opening between the southwest and the northeast of Djibouti, with a strong velocity gradient across the ~12 km wide AG Rift from 0.0 cm yr^{-1} on the southwestern margin to 1.6 cm yr^{-1} on the northeastern margin (Figure 5a). This pattern is consistent with focusing of the far-field Arabia/Somalia divergent motion within the active Quaternary AG Rift [*Vigny et al.*, 2006].

To model deformation across the plate boundary at first order, we use a back slip approach, whereby the plate boundary is locked from the surface to the locking depth and opens freely down to a great depth, assuming an elastic rheology [*Savage*, 1983; *Hofton and Foulger*, 1996] (Figure 7). Prior to modeling, we first subtract a rigid block motion of 1.6 cm yr^{-1} with azimuth N045°E to cancel the large-scale divergence of Arabia and Somalia. Depending on the strike of the dislocation, the strike-slip and closure rates are adjusted accordingly. For clarity, and due to our focus on the deformation across the AG Rift, we do not include in our model the complex structure of the tip of the Aden Ridge, and particularly the presence of numerous N150°E trending faults accommodating the transfer of the extensional deformation between the AG Rift and the Tadjoura Rift [*Manighetti et al.*, 2001]. Therefore, east of the AG Rift, we draw the plate boundary by following the N060°E trending alignment of the aftershocks of the 1978 sequence [*Lépine et al.*, 1980] (Figure 1b). We note that modeling is insensitive to the precise location of the boundary in the Ghoubbet Bay and at the vicinity of

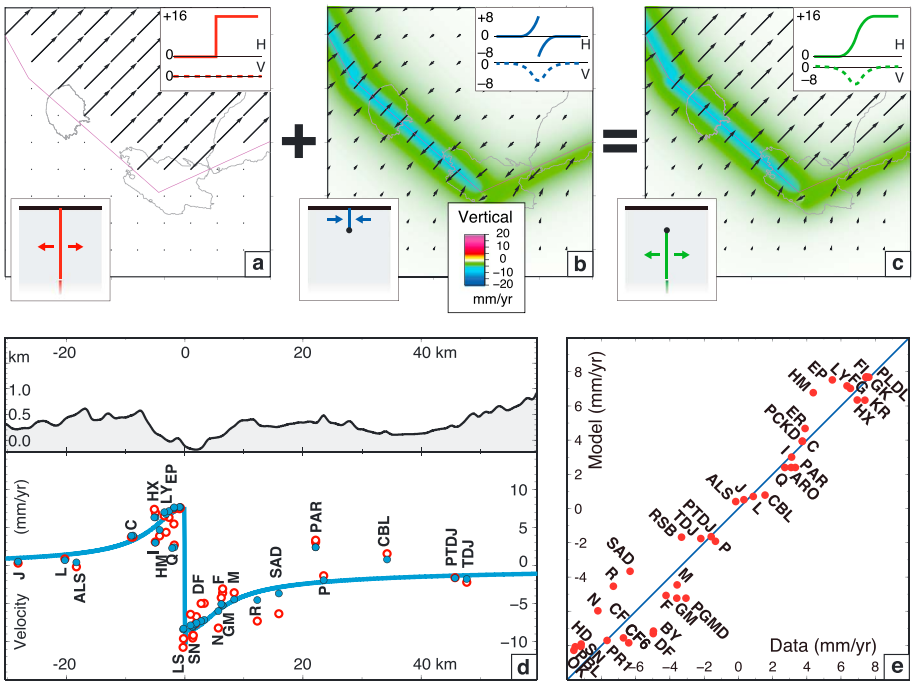

Figure 7. Steady state "interdiking" model of the divergence between Somalia and Arabia plates in the Tadjoura-Asal region. The (c) resulting displacement field is modeled as a sum of (a) a rigid motion of 1.6 cm yr^{-1} along the simplified boundary and (b) a superficial "back slip" from 0 km to a locking depth of 4 km, determined with GPS velocity data (see text)). (d) GPS Velocities (red circles) projected along a N045°E profile (same as Figure 5b) after removing the rigid motion model of 1.6 cm yr^{-1} between Arabia and Somalia plates (Figure 7a). The "back slip" model (Figure 7b) corresponding to the data is calculated at GPS sites (blue dots) and along the N045°E profile (blue line) across the Asal rift (location on Figure 5a). (e) Observed horizontal velocities presented in Figure 7d versus predicted velocities from model (Figure 7b). Unit slope is indicated by dotted line.

the Ghoubbet Pass, since the boundary is entirely located offshore. The actual location of the plate boundary in the interior of the Afar depression is poorly constrained. For simplicity, west of the AG rift, the modeled plate boundary follows the location of active Quaternary faults toward the northwest into the Makkarassou shear zone (Figures 5 and 7a). Again, since our model focuses on the AG Rift, this choice has no impact on the correction that will be applied to postdiking data. In the subaerial part of the AG Rift, the location of this boundary corresponds to the maximum gradient of horizontal GPS velocities. We then invert for the bottom depth of a vertical dislocation, accommodating convergence at a rate of 1.6 cm yr^{-1} in the direction of relative plate motion (Figures 7b and 7d). We find that a locking depth of 4 km explains more than 77% of the data standard deviation, with a RMS below 0.2 cm yr^{-1} (Figures 7d and 7e).

Finally, we use this model (Figure 7c) to remove the steady state component from our horizontal and vertical data. The horizontal motion is corrected by subtracting a slow extension across the rift, with a magnitude everywhere smaller than 1.6 cm yr^{-1}. The strongest corrections concern mainly the benchmarks located far from the rift axis. The vertical motion is corrected by canceling subsidence of the rift axis induced by stretching of the upper crust. The magnitude of the vertical correction is smaller than 1.0 cm yr^{-1} and concerns mainly the benchmarks located at the rift axis.

5.2. Postdiking Period (1978–1991)

5.2.1. Identification of Deformation Sources From Adjusted Vectors

In order to identify the sources involved in the postdiking deformation, we first attempt to retrieve the pattern of horizontal displacement vectors across the rift.

We focus on the two campaigns (1979 and 1984) which include the greatest number of measurements (Figure 2a) and are separated by a time span sufficient to encompass significant displacement. After network adjustment, we correct for the steady state displacements previously estimated from interdiking GPS measurements (section 5.1). However, the network adjustment process is difficult to carry out. Measurements from

the "large-aperture" network are not redundant enough to allow for recovering valid displacement vectors given the small magnitude of the signal (typically ~20 cm change for baseline lengths >10 km in length). As a consequence, only the data from the "intrarift" network, which includes the largest deformation, can be used for the network adjustment. Even so, measurements of the "intrarift" network were performed annually, but partially, and imply that the adjustment is underconstrained. Therefore, assumptions have to be made in order to stabilize the network adjustment process.

The first assumption is to consider that the vertical positions are held fixed, hence leading to a 2-D adjustment only. This is reasonable given that most interstation vectors have small height to length ratios (typically 1:100). Furthermore, we find heuristically that at least one point and one direction have to be held fixed to ensure meaningful network adjustment results. To comply with this requirement, previous works have assumed that two distant points located on the same side of the rift are held fixed ("two-fixed-points" method), implying that the displacement field is cylindrical [*Ruegg et al.*, 1984; *Ruegg and Kasser*, 1987]. We chose to abandon this approach because the postdiking displacement field in both AG Rift and the recently activated Manda Hararo Rift appears to be more complex around the main volcanic center than previously thought. Alternatively, we develop a new strategy, whereby the network adjustment is performed using a single fixed point, while rigid network rotation is a posteriori canceled by holding fixed the direction of relative motion between a pair of well-chosen benchmarks. In contrast with the "two-fixed-points" method, this alternative "one-fixed-point and a rotation" method makes it possible to retrieve the noncylindrical component of motion across the rift (see details in section S2 of the supporting information).

Using the adjusted 1979–1984 horizontal vectors, together with vertical displacements from the 1979–1984 leveling surveys, we perform a nonlinear inversion of the geometry and the volume change of sources of deformation [*Tarantola and Valette*, 1982]. As discussed by *Tarantola et al.* [1980] & *Grandin et al.* [2010b], shallow faulting likely induces a significant component of inelastic deformation that cannot be simply accounted for. Therefore, we do not include faults in the model and we exclude the near-field data prior to any inversion (Figure 4). As explained in section S3 of the supporting information, we test models including only a dike source or a Mogi source (respectively, models "α_D" and "α_M"). Although these two models explain various parts of the observed displacement field, none of them can reproduce the whole data set. Alternatively, the two types of sources (dike and Mogi) are mixed into a hybrid model (model "α_{D+M}") (Figure 8c). The best model includes a Mogi source, located at 5 km of depth below the Fieale caldera with an inflation of 19×10^6 m^3 and a dike-like opening of 8 cm, equivalent to 6×10^6 m^3, between 1979 and 1984. The bottom depth of the dike, which cannot be well constrained due to small aperture of the intrarift network, is held fixed to 4 km. It is consistent with the locking depth deduced from interdiking inversion and corresponds to the brittle-ductile transition determined from microseismic analysis and local tomography [*Doubre et al.*, 2007a, 2007b]. This hybrid source accounts for the predominantly rift-perpendicular orientation of displacement vectors, while simultaneously reproducing the minor radial component visible in the subaerial part of the AG Rift including the inner floor and both of its shoulders. The vertical displacements are also well explained, thereby satisfying the observed horizontal to vertical ratio of surface displacements (Figure 8c). The poor fit of some vectors, especially at the extremities of the network, can be attributed to network adjustment errors due to the redundancy of only few data.

5.2.2. Geometry of the Deformation Sources From Baselines Variations

In section 5.2.1, we identified the two main sources of deformation acting during the postdiking interval (a dike and a Mogi source). However, residual horizontal displacements indicate that the data vectors suffer from a significant degree of incoherence as a result of instability of the network adjustment step. Therefore, the "best" hybrid model, in particular, the precise location of the sources, is likely contaminated by these uncontrolled errors.

In order to achieve a robust geometry of the sources, we directly use the variations of baselines from the two networks over two periods 1979–1984 and 1984–1989, after correcting for the steady state component (section 5.1). Using the baseline variations rather than the vectors avoids the bias arising from an unstable network adjustment procedure. However, it first requires a prior identification of the type and the approximate location of the sources of deformation.

Together with baseline data, we include the leveling observations from the surveys of 1979, 1984, and 2000 in the inversion. No leveling survey was performed in 1989, which makes the baseline and leveling data sets span different time intervals. However, since the overall rate of deformation decreased by a factor of 5 in

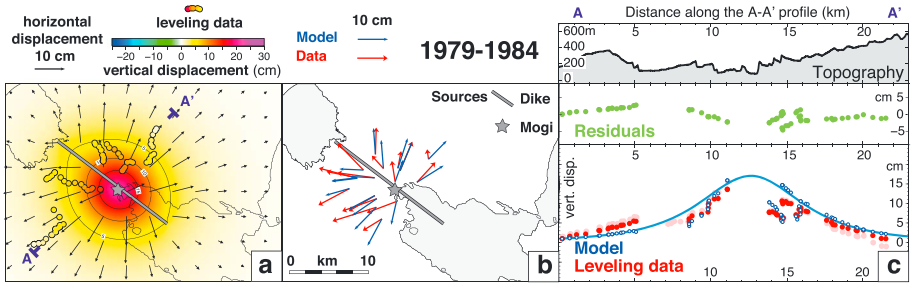

Figure 8. Inversion of the 1979–1984 leveling data and displacement vectors derived from network adjustment based on a combination of a dike and Mogi source (the results of the two inversions based solely on the dike and Mogi sources are presented in Figure S3 in the supporting information). (a) Resulting horizontal (arrows) and vertical (colors) displacement fields obtained from the modeling of a dike segment (grey line) and a Mogi source (grey star). Color-filled circles correspond to observed vertical displacement from leveling data. (b) Horizontal displacements deduced from the network adjustment of the baseline measurements (red arrows) compared to the model (blue arrows). (c) Comparison between observed and modeled vertical displacements projected along N045°E profile. Red circles are the data corrected forming a linear trend used for the inversion, and light pink circles are the original data presented for comparison. The modeled vertical displacements are presented at leveling benchmarks (blue circles) and along the A-A' profile (blue line). Residuals are plotted in green. Topography along the A-A' profile is shown in grey.

1986 (Figures 3b and 4d), displacement in the 1986–2000 time interval should be approximately equal to displacement in the 1984–1986 time interval. Therefore, we use the 1984–2000 leveling data difference to approximate the vertical displacements for the 1984–1989 period, keeping in mind that by doing so the actual displacements are potentially overestimated by a factor of 2.

We invert for the location and inflation of the Mogi source as well as location and opening of the dike using the nonlinear algorithm of *Tarantola and Valette* [1982]. We test the influence of width, strike, length, and depth of the dike and depth of the Mogi point source on the other parameters. We find that the location of the Mogi point source and location, length, and strike of the dike are well constrained. The depth of the top of the dike, although poorly constrained, must be close to the surface. Leveling observations at the rift axis could bring constraints on this parameter, but they are unfortunately strongly affected by faulting processes. For simplicity, we hold the depth of the top of the dike fixed to 0 km (at the surface), which, however, entails a trade-off between this parameter and the amount of opening of the dike: as the top depth varies from 0 to 600 m, opening increases from 8 to 25 cm. Therefore, holding the top depth fixed to 0 km means that the resulting dike opening rates correspond to lower bounds. We also hold the bottom depth of the dike fixed to 4 km. As a result of these uncertainties on the dike depths (top and bottom), the volume of the dike intrusion is poorly constrained. Furthermore, we note that the volume change of the dike affects the determination of the volume change of the Mogi source, since the total volume of the two sources appears to remain nearly constant for a broad range of parameters. Therefore, the volume of the Mogi inflation is also poorly constrained. The depth of the Mogi source lies between 3 and 5 km, implying a volume uncertainty with a factor of 3. Based on geophysical considerations mentioned above, we held the Mogi depth fixed to 5 km, i.e., slightly below the inferred locking depth.

Using the most complete campaigns, we invert the horizontal and vertical displacements for two periods of 5 years. The first period 1979–1984 (model "β_{79-84}" in Table 1 and Figure 9) is the same as previously studied with vectors (section 5.2.1), and the results are similar. For the second period 1984–1989 (model "β_{84-79}" in Table 1 and Figure 10) the data set seems fully explained with only a Mogi source, whereas the dike-like opening component becomes negligible. However, as explained above, since the vertical displacements of the 1984–1989 interval used as input of the inversion are likely overestimated, the results for this period should be regarded with caution. Artificially decreasing the input vertical displacements leads to a reduction of the Mogi component in favor of the dike component. This is explained by the fact that vertical displacements mainly control the Mogi inflation whereas the horizontal extension influences both the dike-like opening and the Mogi source. Overall, despite these trade-offs, we find that location and geometrical parameters of the sources remain stable over the two time intervals.

5.2.3. Time-Based Inversion

In sections 5.2.1 and 5.2.2, we have constrained the geometry and location of the deformation sources using only three campaigns among the data set spanning 10 years of postdiking deformation. However, the

Table 1. Postdiking Model Parameters[a]

	Data Set	Vectors (1979–1984)			Baselines		Temporal (1979–2003)	
	Model	α_D	α_M	α_{D+M}	β_{79-84}	β_{84-89}	$\gamma_{Independent}$	$\gamma_{Combined}$
	Central Easting (UTM, km)	**228.6**		**228.6**	**228.4**	**228.6**	228.7	228.7
	Central Northing (UTM, km)	**1282.5**		**1282.5**	**1281.2**	**1282.5**	1282.6	1282.6
	Z_{top} (km)	0		0	0	0	0	0
Dyke	Width (km)	4		4	4	4	4	4
	Strike (°)	N127°E		N127°E	N127°E	N127°E	N127°E	N127°E
	Length (km)	**21.2**		**17.3**	**23.0**	**24.1**	19.4	19.4
	Opening (cm)	**18.6**		**8.3**	**7.2**	**1.3**	**18.94**[b]	**17.4**[b]
	Volume (10^6 m^3)	**15.8**		**5.7**	**6.6**	**1.2**	**14.7**[b]	**13.5**[b]
	Easting (UTM, km)		**228.2**	**228.2**	**228.3**	**228.2**	228.5	228.5
Mogi	Northing (UTM, km)		**1281.5**	**1281.5**	**1281.5**	**1281.5**	1281.5	1281.5
	Depth (km)		5	5	5	5	5	5
	Volume (10^6 m^3)		**+30**	**+19**	**+22**	**+21**	**+57**[b]	**+55**[b]
	Number of observations	110	110	110	222	152	1769	1769
	Data RMS, vertical only (cm)	5.84	5.84	5.84	6.80	9.30	3.90	3.90
	Residual RMS, vertical only (cm)	3.59	3.77	1.74	1.73	3.75	2.93	3.04
	Data RMS, full data set (cm)	7.56	7.56	7.56	6.09	7.54	8.52	8.52
	Residual RMS, full data set (cm)	3.95	3.9	2.51	2.32	3.02	3.41	3.48

[a]Parameters in bold are determined by the inversion, other parameters are held fixed.
[b]Cumulative 1979–2003.

complete data set encompasses a richer time series that covers the whole decade of the 1980s and provides information on the temporal evolution of activity in the AG Rift over the whole postdiking period.

After holding fixed the geometry of the sources, we conduct a temporal inversion in order to find the evolution of inflation in terms of opening and volume changes for the dike and the Mogi sources. By keeping a fixed geometry, the problem becomes linear. We use directly the baseline variations for the whole time series from the two networks over 1978–2003 periods (after 1990, the data originate from GPS measurements) and leveling data from 1979–1984 to 2000 remeasurements. The assumption of negligible vertical displacements in the 1989–2000 time interval is now eliminated. Prior to inversion, both baseline and leveling data are corrected from the interdiking model in order to remove the steady state component (section 5.1). We describe the inversion method in section S4 of the supporting information.

At this step, we attempted to account for uncertainties in baseline measurements in order to combine the different campaigns and different types of instruments. The formal uncertainties on baseline measurements typically increase with baseline length leading to a significant downweighting of long baselines (≥15 km), which are also fewer in number than the shorter baselines. Hence, the short baselines would dominate the inversion results, thereby exaggerating the importance of shallow sources of deformation comparatively to sources of deformation acting at greater depth. To avoid this bias, we chose uniform uncertainties of 2 cm for all the baseline measurements.

Taking the geometry and locations of the dike and the Mogi sources determined in section 5.2.2, we invert their opening rate independently, using data acquired for each interval of the measurements. A smoothing factor is introduced to control temporal variations of activity.

The optimal model is chosen as a compromise between fit to the data and temporal roughness of the solution using an *L* curve criterion (model "$\gamma_{Independent}$" in Table 1 and Figure 11, open circles). The most striking feature of this model is the similar evolution of the Mogi and dike-like sources, which both exhibit a sudden decrease of the inflation rate in 1985–1986. For the early postdiking period, the rate is $\sim 2 \times 10^6$ m^3 yr^{-1} for the dike-like source and $\sim 4.8 \times 10^6$ m^3 yr^{-1} for the Mogi source. For the second period (after 1986) the rate suddenly decreased for the two sources to nearly zero for the dike and 1.8×10^6 m^3 yr^{-1} for the Mogi source.

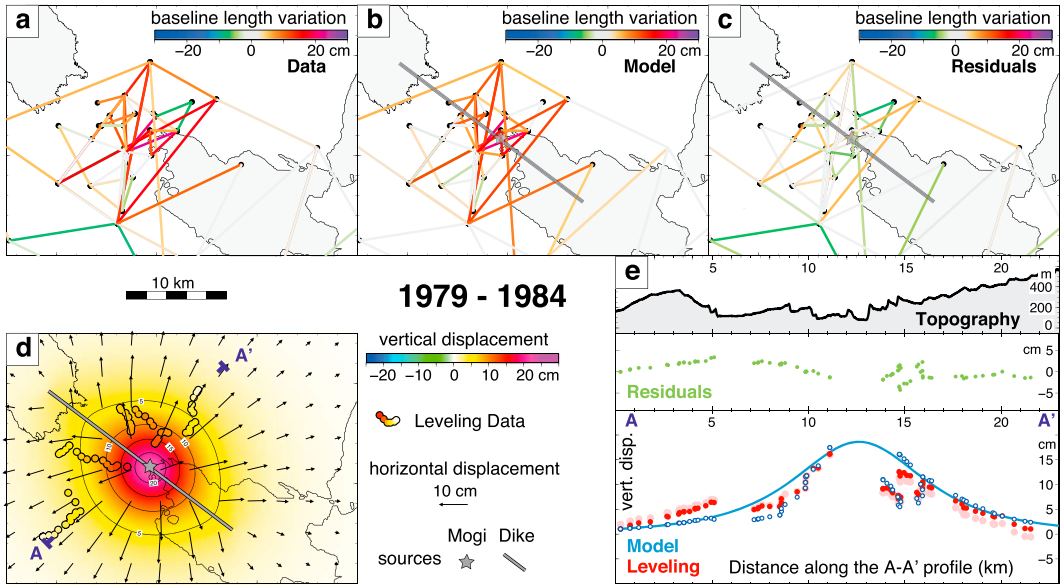

Figure 9. Inversion of the 1979–1984 baselines and leveling measurements. Variations of (a) observed, (b) modeled baseline lengths, and (c) residuals between 1979 and 1984. The line and the star in grey mark the surface projection of the dike segment and the Mogi source, respectively. (d) Resulting horizontal (arrows) and vertical (colors) displacement fields obtained from the modeling of the dike and Mogi sources (in grey). Color-filled circles correspond to observed vertical displacements measured at leveling benchmarks. (e) Comparison between observed and modeled vertical displacements projected along the N045°E profile (A-A' in Figure 9d). Red circles are the data corrected forming a linear trend used for the inversion, and light pink circles are the original data presented for comparison. The modeled vertical displacements are presented at leveling benchmarks (blue circles) and along the A-A' profile (blue line). Residuals are plotted in green. Topography along the A-A' profile is shown in grey.

The similar evolution of the two sources raises a question about the significance of the slight differences between those observed in the second period (i.e., near complete cessation of the dike-like activity versus strong deceleration of the Mogi activity). These minor differences could be attributed to the noise in the data or a trade-off between the sources. To test this hypothesis we propose a simpler model, whereby the two sources are forced to evolve according to the same temporal evolution. Doing so, the number of parameters is reduced by a factor of 2. This is achieved by creating a fictitious source constructed by the superimposition of the Green's functions associated with the two sources, setting the ratio of inflation rates of the two sources to 4. This latter value is estimated by dividing the cumulative volume of the Mogi source by the cumulative volume of the dike from the unconstrained model $\gamma_{\text{Independent}}$. We find that this simpler model (model "γ_{Combined}" in Table 1 and black triangles in Figure 11) does not significantly alter the fit between data and model, suggesting that a common evolution of the two sources cannot be excluded (see section S4). This model also exhibits an evolution in two distinct periods with a major change in 1986 evidenced by the slope break off reflecting a slow down of the inflation and opening of the sources, with dike opening proceeding at 1.7 cm yr^{-1} (1.3×10^6 m^3 yr^{-1}) and inflation of pressure source at 5.5×10^6 m^3 yr^{-1} until 1986, then decreasing to 0.4 cm yr^{-1} (0.3×10^6 m^3 yr^{-1}) and 1.4×10^6 m^3 yr^{-1}, respectively. In all cases, the Mogi source is the main source of deformation after the 1978 dike injection.

5.3. Codiking Period (1973–1978)

In this section, we reinterpret the codiking displacements, taking into account the location and geometry of the sources identified for the postdiking phase. We use data from 1973 and 1979 leveling surveys (vertical displacements) and large-scale geodetic network data (horizontal displacements) from 1973 and 1978–1979. The steady state model presented above is not accounted for in the codiking period, since the steady state displacements between 1973 and 1978 are negligible (<10 cm) compared to the displacements produced by the main 1978 event (> ~100 cm). Furthermore, the uncertainties on the adjusted codiking displacements are larger than the potential correction.

We solve a classical triangulation-trilateration problem with data from the campaign measurements of 1973. We adjust the network with distance measurements from the campaigns of November 1978 and March 1979

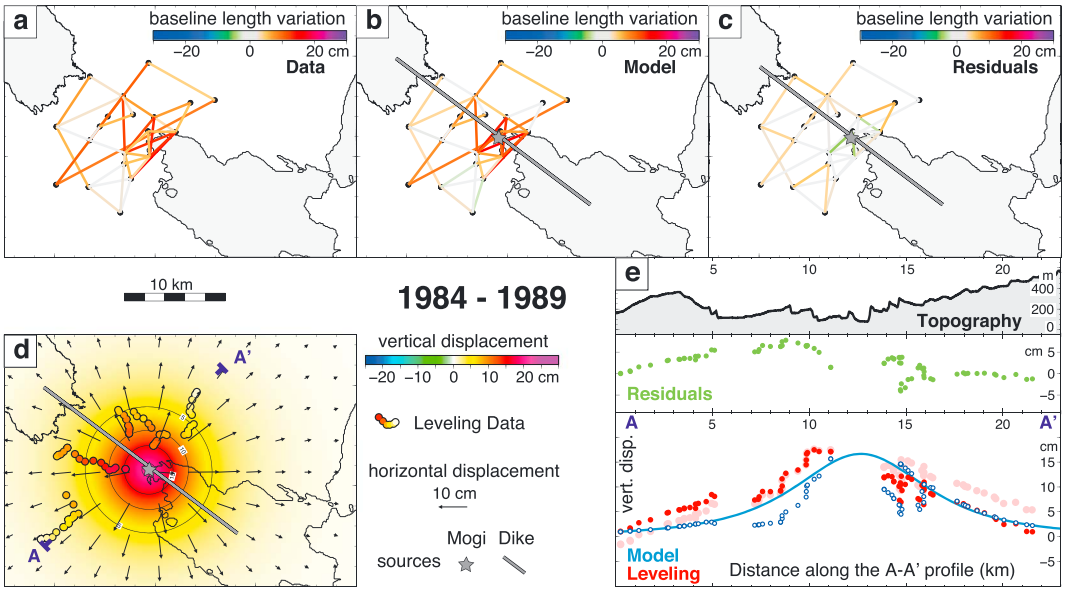

Figure 10. Same as Figure 9 but for the 1984–1989 interval. Note that the 1984–2000 leveling data are used as a proxy for the 1984–1989 vertical displacements (see section 5.2.2 for details).

[*Ruegg et al.*, 1979] (see section S2). Subtraction of the two sets of adjusted benchmark coordinates allows us to deduce the horizontal surface displacements in terms of vectors (Figure 12a, red vectors). The horizontal displacement field displays a dominant N045°E extension pattern across the Ghoubbet Bay, with a maximum amplitude recorded at point N. The very low displacements of points A, U, and V provide constraints on the maximum length of the opening sources.

We compute the difference between the leveling surveys of 1972–1973 and 1978–1979. All the elevation changes are used, except for data at the rift axis showing subsidence induced by faulting (Figure 12b). These benchmarks are all located within the rift inner floor and their subsidence is mainly due to the slip on shallow normal faults [*Rubin and Pollard*, 1988].

Several models have been tested to evaluate the sensitivity of the parameters to the data, introducing progressively more complexity. We first introduce only dike sources (Model A, Table S1). We invert for position,

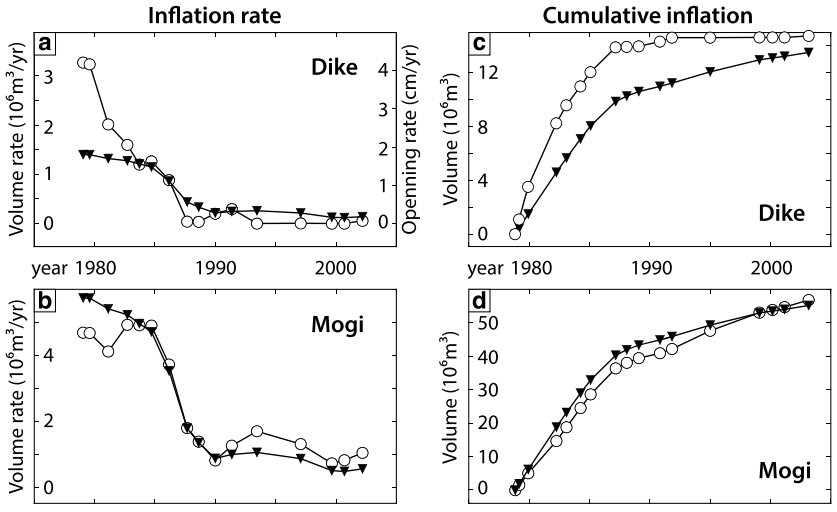

Figure 11. Time-based inversion results. (a, b) The evolution of the inflation rate and (c, d) cumulative volumes for the dike (Figures 11a and 11c) and the Mogi source (Figures 11b and 11d). The white circles show results of the inversion for the unconstrained inversion (i.e., independent sources) and the black triangles for the constrained inversion (i.e., combined evolution of the sources, see text for details).

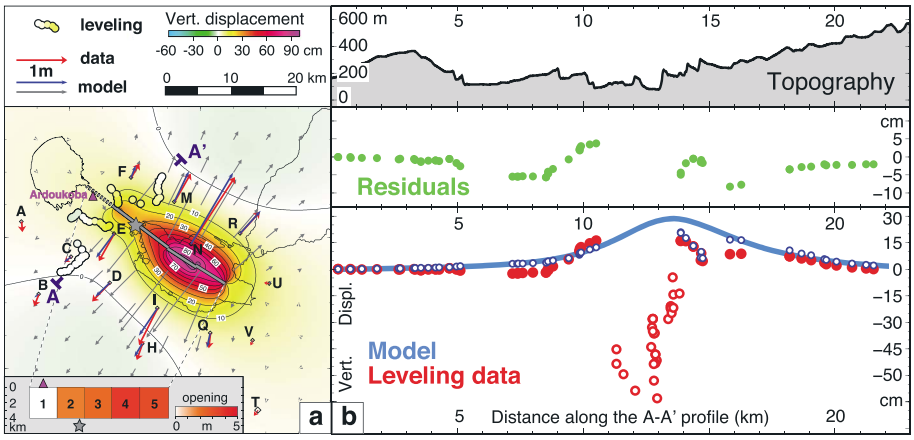

Figure 12. Final 1973–1978 "codiking" model obtained from the inversion of horizontal and vertical data (model D in Table S1 and Table 2). (a) Map of the resulting horizontal (grey arrows) and vertical (with color scale) displacement fields obtained from the modeling of the dike segments (grey lines) and Mogi source (grey star). Red arrows are the horizontal displacements deduced from the network adjustment, blue arrows the model. Color-filled circles correspond to observed vertical displacements from leveling data. The purple triangle represents the location of the Ardoukôba eruption. Inset shows the distribution of opening along the dke segments. (b) Comparison between observed (red circles) and modeled vertical displacements, represented at leveling benchmark (blue circles) and along the A-A' N045°E profile (blue line). Benchmarks located in the inner floor (open red circles) are not used for the inversion. Residuals are plotted in green. Topography along the A-A' profile is shown in grey.

height, length, strike, and opening, setting the parameters step by step. The top and the depth of the dislocation are held fixed to 0 km and 4 km, respectively. The general pattern of opening across the rift is relatively well reproduced by this simple model. However, the model lacks the necessary variability of opening along strike to fit the amplitude and direction of measured displacements. Model B consists of two segments and achieves a better performance in terms of RMS (Table S1). Increasing the number of segments further improves the fit to the data. However, the resolution of the data imposes a limitation of the number of segments that can reasonably be included in the model. We find that a model consisting of five dike segments is an effective compromise between performance and simplicity. We note that the five segments correspond to the mesh of the geodetic network, which is shaped in its central part by the five baselines carrying the largest part of the codiking signal (from west to east: C-F, E-F, D-M, I-N, and Q-R, see Figures 3a and 12a). This means that our data set is unable to resolve details of the dike opening at a scale smaller than 5 km. Therefore, using five segments, we invert the opening, holding fixed the location and geometry of the three northwestern dike segments (subaerial part of the rift) to be consistent with that obtained for the postdiking period, and adjusting the strike

Table 2. Codiking Model Parameters for Model D (Table S1 and Figure 12)[a]

	Segment	1	2	3	4	5
	Central Easting (UTM, km)	241.5	237.1	233.0	228.8	224.6
	Central Northing (UTM, km)	1274.3	1276.9	1280.0	1283.1	1286.3
	Z_{top} (km)	0	0	0	0	0
Dyke	Width (km)	4	4	4	4	4
	Strike (°)	53	53	53	53	53
	Length (km)	5.2	5.2	5.2	5.2	5.2
	Opening (cm)	**315**	**383**	**218**	**174**	**0**
	Volume (10^6 m^3)	**65**	**80**	**22**	**36**	**0**
	Easting (UTM, km)			229.1		
Mogi	Northing (UTM, km)			1281.3		
	Depth (km)			5		
	Volume (10^6 m^3)			**−28**		

[a]Parameters in bold are determined by the inversion, other parameters are held fixed.

and position of the two southeastern segments (in the Ghoubbet Bay) by trial and error (Table S1, model C). The width of the dike segments is still held fixed from 0 to 4 km depth. The strike of the two segments within the Ghoubbet Bay is rotated in agreement with the slight change of strike of the plate boundary toward the Ghoubbet Pass revealed by the alignment of the aftershocks of the 1978 sequence (Figure 1b). However, this model consisting only in dike segments systematically generates unacceptable uplift and insufficient extension. Changing the geometrical parameters of the dike does not improve the discrepancy between observed and modeled vertical/horizontal displacement ratio.

In agreement with our results from the postdiking phase (section 5.2), which require the presence of a crustal midsegment magma chamber feeding the dike intrusion, we introduce a Mogi source in deflation in the codiking model. The final model includes both a segmented dike and a pressure source (Table S1, model D). We hold fixed the geometrical parameters (length, width, strike, and location) and invert for the opening of the dislocations and the volume decrease within the Mogi source. Due to the sparseness of the data near the Fieale caldera, location of the Mogi source cannot be resolved with accuracy. For consistency, we use the location obtained from the postdiking modeling below the Fieale caldera (section 5.2.2).

Our final model (Figure 12) consists of a 21 km long and 4 km high dike that opens from 1.7 to 3.8 m without a gap accounting for a total volume of $226 \times 10^6 m^3$, and a 5 km deep reservoir below the Fieale caldera with a deflation of $28 \times 10^6 m^3$. Figure 12 shows the fit with the observations for both horizontal and vertical displacements. The model satisfactorily explains the elastic rebound perpendicular to the rift axis as well as the along-axis elevation changes sampled by the sinuous leveling line (Figure 12b, blue dots). The above volume estimates should, however, be regarded with caution. Since the "codiking" period actually includes a few months of postdiking activity, which is mainly characterized by a global inflation of the rift, the actual deflation associated with the dike intrusion event may have been partly compensated by early postdiking reinflation taking place before the first postdiking survey. Nevertheless, the observation that retrieved dike opening becomes continuous along the rift when a deflating source is placed below the Fieale caldera (i.e., the opening gap at midsegment vanishes) is interpreted as a sign of coherence of this hybrid model, as discussed below.

6. Discussion

6.1. An Active Central Magma Reservoir Below the AG Rift

In this paper, we analyze and model all the geodetic data acquired during and after the 1978 rifting event to identify the magma source involved in feeding the dike. We assume that, in the decades following the 1978 event, deformation has evolved in response to transient volume/pressure changes within the central plumbing center, superimposed onto a large-scale steady state loading process of the plate boundary. By substracting a steady state deformation field derived from the GPS velocities over the 1999–2014 period, we isolate the transient component of postdiking deformation which is interpreted as reflecting the combined action of (1) a conventional pressure source below the Fieale caldera, modeled as Mogi source, and (2) a significant component of rift-perpendicular dilation, modeled as a dike segment.

The influence of pressure sources in postdiking contexts has already been underlined for other rifting events. In the case of the 1974–1985 Krafla rifting episode (Iceland), short subsidence signals of Krafla central volcano coeval with sudden dike intrusions, followed by periods of slow, continuous uplift [*Björnsson*, 1985; *Árnadóttir et al.*, 1998] were clear enough to evidence pressure changes within a magma chamber and point out its role as a central source feeding most of the dike intrusions.

In the case of the Manda Hararo-Dabbahu episode, the signature of a midsegment magma reservoir in the InSAR data covering the main September 2005 dike intrusion could not be identified unambiguously. Likely due to the superimposition of shallow inflation of the dike and deep deflation of the magma source, a gap in the along-axis opening distribution of the dike appeared in the middle of the segment [*Wright et al.*, 2006; *Grandin et al.*, 2009]. Migration of seismicity during subsequent dike injections followed by short inflation transients allowed for identifying the location of a central source feeding the rift with fresh magma [*Keir et al.*, 2009; *Belachew et al.*, 2011; *Hamling et al.*, 2009; *Grandin et al.*, 2010b, 2011; *Hamling et al.*, 2014]. An account of the potential deflation of this inferred magma source in a codiking model of the main September 2005 dike intrusion allows for the imaging of a continuous dike body below the rift segment, thereby reestablishing hydraulic connectivity [*Wright et al.*, 2006; *Grandin et al.*, 2009].

Our interpretation of deformation in the AG Rift follows a similar logic. The previously published codiking model [*Tarantola et al.*, 1979, 1980] consisted of two separate dike segments, with an estimated total volume of intruded material of 200×10^6 m^3. Adding a deflation component solves the problem of continuity of dike opening in our model. Furthermore, the Ardoukôba eruption corresponds to the intersection of the dike with the rift surface and its location coincides with the dike termination, similar to three intrusions during the Manda Hararo rifting episode (2005–2010) [*Grandin et al.*, 2010b; *Barnie et al.*, 2015] and during the Bárdarbunga intrusion in Iceland (2014) [*Sigmundsson et al.*, 2014]. Eruptions fed by dikes emplaced laterally also often correspond to the tip of the dike in conventional volcanic environments [*Bonaccorso et al.*, 2002; *Peltier et al.*, 2005; *Lundgren et al.*, 2013]. By analogy, the locations of the observed Ardoukôba eruption site and its infered feeder dike therefore seem coherent.

A body of geophysical observations point to the existence of an active magma reservoir below the Fieale caldera (section 2.1). Our results further suggest that the Fieale midsegment reservoir may have evolved to become the main feeding source of the recent intrusive and effusive activity in AG Rift and, in particular, of the dike injection in 1978.

An open question remains regarding the origin of the fast opening component observed during the postdiking period in the AG Rift. A similar component of dilation was clearly observed by InSAR following the 2005 Manda Hararo megadike intrusion [*Grandin et al.*, 2010a; *Hamling et al.*, 2014; *Pagli et al.*, 2014], where the aseismic and fast-slipping faults during the few months following the main dike intrusion have been interpreted as the result of a migration of magma to shallower depths [*Dumont et al.*, 2016]. Even if the data set in the AG Rift is not rich enough to postulate with no ambiguity for a similar process, we consider that the observed nonradial component of deformation centered along the rift axis is related to the slow inflation of pervasive rift-parallel cracks connected to the replenishing central magma reservoir rather than to a series of planar intrusions into the inner floor. Indeed, the temporal evolution of the seismicity during the postdiking period does not show any strong burst or epicenter alignment for the 1979–1986 period that would be characteristic of dike intrusion [e.g., *Rubin and Gillard*, 1998]. Moreover, during this time span, the lack of abrupt changes in the geodetic time series seems to confirm a continuous deformation following the 1978 dike, which is smaller than the first intrusions of the rifting episodes in the Manda Hararo and Krafla segments. Although the space coverage of the tomographic image obtained for the subaerial part of the rift is limited, a fully molten medium, or a massive intrusion can be excluded [*Doubre et al.*, 2007a]. Alternatively, the medium may consist of a crystal-melt-gas mush behaving plastically at a time scale of months to years. An aqueous component, such as a hydrothermal brine, may also play a role at shallow depth [*Doubre et al.*, 2007a].

6.2. Relevance of Viscoelastic Relaxation Processes

Our model is based on the interpretation that postdiking deformation results from active magmatic phenomena possibly related to a component of hydrothermal activity. Alternative processes of deformation could be invoked to explain the observations, such as viscoelastic relaxation in the lower crust or upper mantle. This latter process has been previously proposed to explain postdiking deformation [*Vigny et al.*, 2007; *Hofton and Foulger*, 1996; *Nooner et al.*, 2009], especially when the deformation follows a smooth evolution. Here the opposite approach was adopted. We used an elastic rheology to determine the time evolution of the deformation source. This choice was mainly based on the fact that in the Ghoubbet Bay, the area affected by the largest codiking opening, little or no postdiking extension occurs. In contrast, intense deformation is detected in the subaerial part of the AG Rift, especially near the Fieale caldera.

This observation is at odds with a viscoelastic interpretation of postdiking deformation. Indeed, assuming a simple 1-D viscoelastic structure, relaxation models systematically predict that the response to a stress perturbation should roughly take place at the location of the maximum initial stress perturbation. In the case of postdiking relaxation models, maximum codiking opening and maximum postdiking response should coincide spatially [e.g., *Foulger et al.*, 1992; *Hofton and Foulger*, 1996; *Nooner et al.*, 2009], which is inconsistent with our observations. If viscoelastic relaxation were a dominant process during the postdiking period, one would expect maximum postdiking deformation to take place in the Ghoubbet area, where the maximum codiking deformation was observed. Therefore, this suggests that viscoelastic deformation likely plays a minor role during the postdiking period, thereby favoring magmatic processes as the primary cause of observed deformation. Nevertheless, viscoelastic relaxation cannot be totally discounted, in particular, as the potentially complex 3-D shape of the brittle-elastic interface [e.g., *Pedersen et al.*, 2009; *Grandin et al.*, 2012] may be expected to induce a focusing of postdiking deformation toward the segment center.

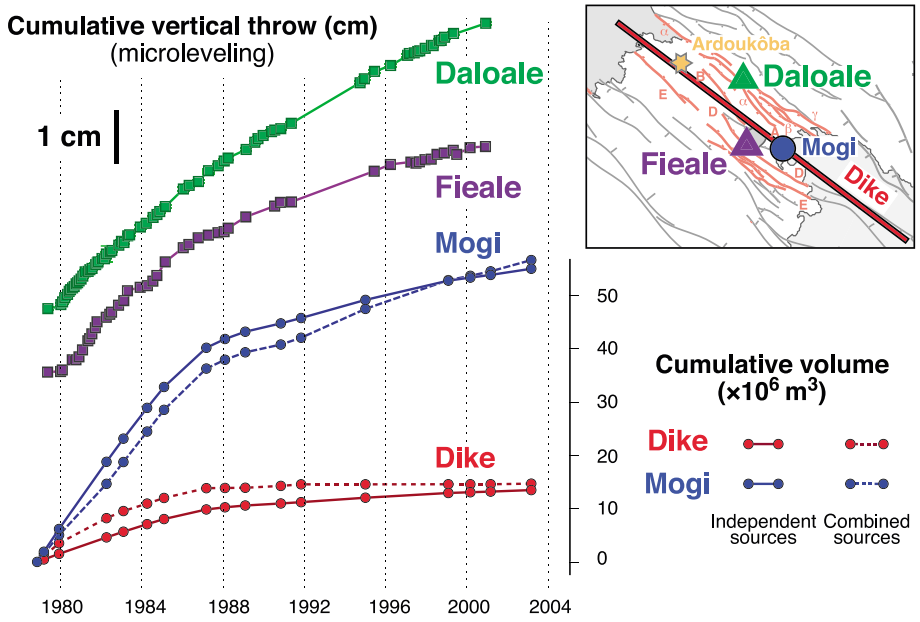

Figure 13. Results of the time-based inversion (Figure 11) compared to vertical throw across fault "D" in the Fieale area (purple) and fault "γ" in the Daloale area (green) [*Ruegg et al.*, 1984; *Stein et al.*, 1991], with location of the two microleveling sites plotted with the same colors in the inset.

A second argument against the prevalence of viscoelastic relaxation processes comes from the temporal evolution of the deformation reconstructed from the full inversion of the whole data set. As already noted by *Cattin et al.* [2005], a sharp change in the observed velocities is inferred around 1986, with a sixfold decrease of deformation rate taking place in less than 1 year. Our exhaustive analysis of the baselines and leveling data confirms that this change represents a global feature of the data set and is unlikely to be an artifact resulting from noise in an individual time series of measurements. Such a spectacular change in velocity would be consistent with an active process and suggests that the magmatic activity is the source of deformation. Indeed, similarly sudden changes of strain rates taking place over the course of a few months are detected by geodetic observations in numerous conventional volcanic environments (i.e., not associated with a plate boundary) such as Kilauea volcano [e.g., *Dvorak and Dzurisin*, 1993; *Baker and Amelung*, 2012], Yellowstone [e.g., *Chang et al.*, 2010], Campi Flegrei [e.g., *Del Gaudio et al.*, 2010], or Long Valley caldera [e.g., *Tizzani et al.*, 2009]. These changes are commonly interpreted as reflecting a modification in the supply rate to the shallow part of the plumbing system, potentially influenced by closure or opening of magma pathways. On the other hand, viscoelastic relaxation processes typically exhibit a smooth temporal evolution, generally modeled by simple exponential or logarithmic functions. If nonlinear viscoelasticity is invoked to reproduce the abrupt slow down in 1985, an extremely high nonlinearity would certainly be required. This would become a very complex scenario, best to be avoided. The change of surface velocities in 1986 in the AG Rift therefore argues in favor of the magmatic origin of postdiking deformation.

Microleveling on some of the most active faults in the AG Rift has been carried out with monthly measurements after the 1978 dike intrusion, revealing significant creep at the surface. One survey was performed near Fieale, right above the inferred source of midsegment inflation [*Ruegg et al.*, 1984] (Figure 13). A similar drop in the creep rate can be inferred around 1986, although the variation seems to be somehow smoother. We note that creep data was not used in our analysis. Nevertheless, the striking resemblance between the evolution of activity of the main source of large-scale deformation, on one hand, and temporal variations of local creep rate at Fieale caldera, on the other, strongly suggest a common causal relationship. Shallow creep at the surface seems to mimic deep sources of deformation. This similar evolution likely reflects the passive response of faults to the forcing exerted by magmatic sources below the Fieale caldera, as proposed by *Doubre and Peltzer* [2007]. The same conclusions were drawn from an InSAR study of postdiking deformation in the Manda Hararo Rift [*Dumont et al.*, 2016]. The common evolution of creep and inferred inflation of the Fieale magma reservoir further reinforce the primarily magmatic origin of postdiking deformation in the AG Rift.

7. Conclusion

In this paper, we analyzed 40 years of geodetic data acquired in the Asal-Ghoubbet (AG) Rift. These observations have recorded the deformation produced by the rifting event of November 1978 and extend throughout the subsequent postrifting period. This data set has never been exploited comprehensively. We propose a coherent scenario in terms of geometry and temporal evolution of the deformation sources for the whole 1978–2014 period.

The 1978 event is modeled as a 226×10^6 m^3 dike intrusion emplaced along the subaerial part of the AG Rift and below the Ghoubbet Bay. Unlike previous models [*Tarantola et al.*, 1979, 1980], we also include a deflating pressure source to the codiking model, accounting for a deflation of at least -28×10^6 m^3. This pressure source is located below the Fieale caldera, a volcanic edifice dismantled by tectonic activity since ~100 ka. Including this deflating component allows for connecting the whole dike body, which would otherwise be segmented in two hydraulically disconnected parts. We propose that this pressure source represents the central midsegment magma reservoir that fed the 1978 dike and associated eruption of Ardoukôba.

Furthermore, we explain postdiking deformation with a two-component source. The predominantly radial displacement pattern is modeled by the inflation of the pressure source below the Fieale caldera involved during the diking event, with a cumulative inflation of $+55 \times 10^6$ m^3. In addition, an extensional dike-like source is included to account for residual rift-perpendicular dilation taking place mainly at the vicinity of the central magma reservoir below the subaerial part of the rift.

By using the complete data set covering the 25 year period of postdiking, with particular focus on relative distance measurements carried out on a yearly basis across and along the AG Rift, we invert for the temporal evolution of the activity of these two sources. The rapid change in deformation rates observed around 1986 is associated with a substantial slow down of the inflation rate of both sources. As the two sources follow similar time behavior, a conjoint evolution of the two sources cannot be excluded. This may suggest that isotropic inflation and dike-like dilation respond to a single underlying process. Temporal variation in the magma supply rate to the shallow part of the AG Rift plumbing system is likely to explain the spectacular change of deformation rates observed in 1986.

Finally, we highlight the prevalence of magmatic activity in the 10 years following the 1978 dike intrusion, rather than viscoelastic relaxation. These results indicate that both the mode and the rate of deformation in the AG Rift are controlled by the availability of magma at shallow depth over a broad range of time scales (1–10^5 years).

Acknowledgments

This work has been made possible, thanks to the partnership between the Centre d'Étude et de Recherche de Djibouti (CERD) and Institut de Physique du Globe de Paris (IPGP), through the common management of Arta Geophysical Observatory (OGA) which have allowed for acquiring more than 40 years of seismic and geodetic data. The Institut Français of the French Embassy in Djibouti has supported the OGA since its foundation in 1973. We thank all the teams that have succeeded each another over the years to manage the observatory, install, maintain, and monitor stations, and all the scientists that have participated in data acquisition campaigns. The Afar programs have been historically sponsored by INSU/CNRS (Tectoscope, Idhil, IT, ACI...), and more recently by ANR "DoRA" (ANR-09-JCJC-0051-01). Recent campaigns used services of French INSU-CNRS GPS instrument pool (now RESIF). This paper has benefited from fruitful discussions with Jean-Claude Ruegg (IPGP), Pierre Briole (ENS), and A. Coulomb (IGN), who acquired most of the baseline measurements and leveling data and shared their expertise in analysis and processing. We also thank Gilles Peltzer for sharing results and providing constructive comments on the present day deformation in the Asal rift. This is IPGP contribution number 3767. The data for this paper are available by contacting the corresponding author at delphine.smittarello@ens.fr.

References

Abdallah, A., V. Courtillot, M. Kasser, A.-Y. Le Dain, J.-C. Lépine, B. Robineau, J.-C. Ruegg, P. Tapponnier, and A. Tarantola (1979), Relevance of Afar seismicity and volcanism to the mechanics of accreting plate boundaries, *Nature*, *282*(5734), 17–23.

Allard, P., and H. Tazieff (1979), Observations of seafloor spreading in Afar during the November 1978 fissure eruption, *Nature*, *279*, 30–33.

Árnadóttir, T., F. Sigmundsson, and P. T. Delaney (1998), Sources of crustal deformation associated with the Krafla, Iceland, eruption of September 1984, *Geophys. Res. Lett.*, *25*(7), 1043–1046.

Audin, L., I. Manighetti, P. Tapponnier, F. Métivier, E. Jacques, and P. Huchon (2001), Fault propagation and climatic control of sedimentation on the Ghoubbet rift floor: Insights from the Tadjouraden cruise in the western Gulf of Aden, *Geophys. J. Int.*, *144*(2), 391–413.

Baker, S., and F. Amelung (2012), Top-down inflation and deflation at the summit of Kīlauea Volcano, Hawai'i observed with InSAR, *J. Geophys. Res.*, *117*, B12406, doi:10.1029/2011JB009123.

Ballu, V., M. Diament, P. Briole, and J.-C. Ruegg (2003), 1985–1999 gravity field variations across the Asal Rift: Insights on vertical movements and mass transfer, *Earth Planet. Sci. Lett.*, *208*(1), 41–49.

Barnie, T., et al. (2015), A multidisciplinary study of the final episode of the Manda Hararo dike sequence, Ethiopia, and implications for trends in volcanism during the rifting cycle, in *Magmatic Rifting and Active Volcanism*, edited by T. J. Wright et al., *Geol. Soc. London, Spec. Publ., 420*, SP420–6.

Bekoa, A. (1986), Modélisations des déformations en milieu volcanique: Application, rift d'Asal(Djibouti), PhD thesis, University Pierre et Marie Curie - Paris VI, Paris, France.

Belachew, M., C. Ebinger, D. Coté, D. Keir, J. Rowland, J. Hammond, and A. Ayele (2011), Comparison of dike intrusions in an incipient seafloor-spreading segment in Afar, Ethiopia: Seismicity perspectives, *J. Geophys. Res.*, *116*, B06405, doi:10.1029/2010JB007908.

Björnsson, A. (1985), Dynamics of crustal rifting in NE Iceland, *J. Geophys. Res.*, *90*(B12), 10,151–10,162.

Bonaccorso, A., M. Aloisi, and M. Mattia (2002), Dike emplacement forerunning the Etna July 2001 eruption modeled through continuous tilt and GPS data, *Geophys. Res. Lett.*, *29*(13), 1624, doi:10.1029/2001GL014397.

Buck, W. R., P. Einarsson, and B. Brandsdóttir (2006), Tectonic stress and magma chamber size as controls on dike propagation: Constraints from the 1975–1984 Krafla rifting episode, *J. Geophys. Res.*, *111*, B12404, doi:10.1029/2005JB003879.

Callot, J.-P., L. Geoffroy, C. Aubourg, J. Pozzi, and D. Mege (2001), Magma flow directions of shallow dykes from the East Greenland volcanic margin inferred from magnetic fabric studies, *Tectonophysics*, *335*(3), 313–329.

Cattin, R., C. Doubre, J.-B. De Chabalier, G. King, C. Vigny, J.-P. Avouac, and J.-C. Ruegg (2005), Numerical modelling of quaternary deformation and post-rifting displacement in the Asal–Ghoubbet rift (Djibouti, Africa), *Earth Planet. Sci. Lett.*, *239*(3), 352–367.

Chang, W.-L., R. B. Smith, J. Farrell, and C. M. Puskas (2010), An extraordinary episode of Yellowstone caldera uplift, 2004–2010, from GPS and InSAR observations, *Geophys. Res. Lett.*, *37*, L23302, doi:10.1029/2010GL045451.

De Chabalier, J.-B., and J.-P. Avouac (1994), Kinematics of the Asal Rift (Djibouti) determined from the deformation of Fieale volcano, *Science*, *265*, 1677–1677.

de Vries, B. V. W., and O. Merle (1996), The effect of volcanic constructs on rift fault patterns, *Geology*, *24*(7), 643–646.

Del Gaudio, C., I. Aquino, G. Ricciardi, C. Ricco, and R. Scandone (2010), Unrest episodes at Campi Flegrei: A reconstruction of vertical ground movements during 1905–2009, *J. Volcanol. Geotherm. Res.*, *195*(1), 48–56.

Delaney, P., D. Pollard, J. Ziony, and E. McKee (1986), Field relations between dikes and joints: Emplacement processes and paleostress analysis, *J. Geophys. Res.*, *91*, 4920–4938.

Déprez, A., C. Doubre, F. Masson, and P. Ulrich (2013), Seismic and aseismic deformation along the East African Rift System from a reanalysis of the GPS velocity field of Africa, *Geophys. J. Int.*, *193*(3), 1353–1369.

Déprez, A., C. Doubre, F. Masson, and P. Ulrich (2015), Erratum: Seismic and aseismic deformation along the East African Rift System from a reanalysis of the GPS velocity field of Africa, *Geophys. J. Int.*, *200*(1), 556–556.

Doubre, C., and L. Geoffroy (2003), Rift-zone development around a plume-related magma centre on the Isle of Skye (Scotland): A model for stress inversions, *Terra Nova*, *15*(4), 230–237.

Doubre, C., and G. Peltzer (2007), Fluid-controlled faulting process in the Asal Rift, Djibouti, from 8 yr of radar interferometry observations, *Geology*, *35*(1), 69–72.

Doubre, C., I. Manighetti, C. Dorbath, L. Dorbath, E. Jacques, and J. Delmond (2007a), Crustal structure and magmato-tectonic processes in an active rift (Asal-Ghoubbet, Afar, East Africa): 1. Insights from a 5-month seismological experiment, *J. Geophys. Res.*, *112*, B05405, doi:10.1029/2005JB003940.

Doubre, C., I. Manighetti, L. Dorbath, C. Dorbath, D. Bertil, and J. Delmond (2007b), Crustal structure and magmato-tectonic processes in an active rift (Asal-Ghoubbet, Afar, East Africa): 2. Insights from the 23-year recording of seismicity since the last rifting event, *J. Geophys. Res.*, *112*, B05406, doi:10.1029/2006JB004333.

Dumont, S., A. Socquet, R. Grandin, C. Doubre, and Y. Klinger (2016), Surface displacements on faults triggered by slow magma transfers between dyke injections in the 2005–2010 rifting episode at Dabbahu–Manda–Hararo rift (Afar, Ethiopia), *Geophys. J. Int.*, *204*(1), 399–417.

Dvorak, J. J., and D. Dzurisin (1993), Variations in magma supply rate at Kilauea volcano, Hawaii, *J. Geophys. Res.*, *98*(B12), 22,255–22,268.

Dzurisin, D. (2007), Classical surveying techniques, in *Volcano Deformation*, edited by P. Blondel, pp. 33–80, Springer, Berlin.

Ebinger, C., and M. Casey (2001), Continental breakup in magmatic provinces: An Ethiopian example, *Geology*, *29*(6), 527–530.

Einarsson, P. (1991), Earthquakes and present-day tectonism in Iceland, *Tectonophysics*, *189*(1), 261–279.

Fialko, Y. A., and A. M. Rubin (1998), Thermodynamics of lateral dike propagation: Implications for crustal accretion at slow spreading mid-ocean ridges, *J. Geophys. Res.*, *103*(B2), 2501–2514.

Foulger, G., C. Jahn, G. Seeber, P. Einarsson, B. Julian, and K. Heki (1992), Post-rifting stress relaxation at the divergent plate boundary in northeast Iceland, *Nature*, *358*(6386), 488–490.

Gasse, F., and J.-C. Fontes (1989), Palaeoenvironments and palaeohydrology of a tropical closed lake (Lake Asal, Djibouti) since 10,000 yr BP, *Palaeogeogr. Palaeoclimatol. Palaeoecol.*, *69*, 67–102.

Grandin, R., et al. (2009), September 2005 Manda Hararo-Dabbahu rifting event, Afar (Ethiopia): Constraints provided by geodetic data, *J. Geophys. Res.*, *114*, B08404, doi:10.1029/2008JB005843.

Grandin, R., A. Socquet, M.-P. Doin, E. Jacques, J.-B. de Chabalier, and G. King (2010a), Transient rift opening in response to multiple dike injections in the Manda Hararo rift (Afar, Ethiopia) imaged by time-dependent elastic inversion of interferometric synthetic aperture radar data, *J. Geophys. Res.*, *115*, B09403, doi:10.1029/2009JB006883.

Grandin, R., A. Socquet, E. Jacques, N. Mazzoni, J.-B. de Chabalier, and G. King (2010b), Sequence of rifting in Afar, Manda-Hararo rift, Ethiopia, 2005–2009: Time-space evolution and interactions between dikes from interferometric synthetic aperture radar and static stress change modeling, *J. Geophys. Res.*, *115*, B10413, doi:10.1029/2009JB000815.

Grandin, R., E. Jacques, A. Nercessian, A. Ayele, C. Doubre, A. Socquet, D. Keir, M. Kassim, A. Lemarchand, and G. King (2011), Seismicity during lateral dike propagation: Insights from new data in the recent Manda Hararo–Dabbahu rifting episode (Afar, Ethiopia), *Geochem. Geophys. Geosyst.*, *12*, Q0AB08, doi:10.1029/2010GC003434.

Grandin, R., A. Socquet, C. Doubre, E. Jacques, and G. C. King (2012), Elastic thickness control of lateral dyke intrusion at mid-ocean ridges, *Earth Planet. Sci. Lett.*, *319*, 83–95.

Hamling, I. J., A. Ayele, L. Bennati, E. Calais, C. J. Ebinger, D. Keir, E. Lewi, T. J. Wright, and G. Yirgu (2009), Geodetic observations of the ongoing Dabbahu rifting episode: New dyke intrusions in 2006 and 2007, *Geophys. J. Int.*, *178*(2), 989–1003.

Hamling, I. J., T. J. Wright, E. Calais, L. Bennati, and E. Lewi (2010), Stress transfer between thirteen successive dyke intrusions in Ethiopia, *Nat. Geosci.*, *3*(10), 713–717.

Hamling, I. J., T. J. Wright, E. Calais, E. Lewi, and Y. Fukahata (2014), InSAR observations of post-rifting deformation around the Dabbahu rift segment, Afar, Ethiopia, *Geophys. J. Int.*, *197*(1), 33–49.

Hayward, N., and C. Ebinger (1996), Variations in the along-axis segmentation of the Afar rift system, *Tectonics*, *15*(2), 244–257.

Heki, K., G. Foulger, B. Julian, and C.-H. Jahn (1993), Plate dynamics near divergent boundaries: Geophysical implications of postrifting crustal deformation in NE Iceland, *J. Geophys. Res.*, *98*(B8), 14,279–14,297.

Hofton, M., and G. Foulger (1996), Postrifting anelastic deformation around the spreading plate boundary, north Iceland, 1. Modeling of the 1987–1992 deformation field using a viscoelastic Earth structure, *J. Geophys. Res.*, *101*, 25–403.

IGN, et al. (1973), Implantation d'un réseau géodésique pour la mesure directe de l'expansion d'un rift océanique – Participation de l'IGN à la RCP 180 – Territoire français des Afars et des Issas, *Tech. Rep.*, IGN.

Jestin, F., P. Huchon, and J. Gaulier (1994), The Somalia plate and the East African rift system: Present-day kinematics, *Geophys. J. Int.*, *116*(3), 637–654.

Kasser, M., J.-C. Ruegg, and J.-C. Lepine (1987), Geodetic measurements on the Asal Rift (Djibouti): Twelve years of observations, *J. Geodyn.*, *7*(3), 221–226.

Keir, D., et al. (2009), Evidence for focused magmatic accretion at segment centers from lateral dike injections captured beneath the Red Sea rift in Afar, *Geology*, *37*(1), 59–62.

Le Dain, A.-Y., B. Robineau, and P. Tapponnier (1980), Les effets tectoniques de l'événement sismique et volcanique de Novembre 1978 dans le rift d'Asal-Ghoubbet, *Bull. Soc. Geol. Fr.*, *22*(6), 817–822.

Lépine, J.-C., J.-C. Ruegg, and A.-M. Anis (1980), Sismicité du rift d'Asal-Ghoubbet pendant la crise sismo-volcanique de Novembre 1978, *Bull. Soc. Geol. Fr.*, *22*(6), 809–816.

Lundgren, P., et al. (2013), Evolution of dike opening during the March 2011 Kamoamoa fissure eruption, kīlauea volcano, hawaii, *J. Geophys. Res. Solid Earth*, *118*, 897–914, doi:10.1002/jgrb.50108.
Manighetti, I., P. Tapponnier, P. Gillot, E. Jacques, V. Courtillot, R. Armijo, J.-C. Ruegg, and G. King (1998), Propagation of rifting along the Arabia-Somalia plate boundary: Into Afar, *J. Geophys. Res.*, *103*(B3), 4947–4974.
Manighetti, I., P. Tapponnier, V. Courtillot, Y. Gallet, E. Jacques, and P.-Y. Gillot (2001), Strain transfer between disconnected, propagating rifts in Afar, *J. Geophys. Res.*, *106*(B7), 13,613–13,665.
Medynski, S., et al. (2016), Magmatic cycles pace tectonic and morphological expression of rifting (Afar depression, Ethiopia), *Earth Planet. Sci. Lett.*, *446*, 77–88.
Nooner, S. L., L. Bennati, E. Calais, W. R. Buck, I. J. Hamling, T. J. Wright, and E. Lewi (2009), Post-rifting relaxation in the Afar region, Ethiopia, *Geophys. Res. Lett.*, *36*, L21308, doi:10.1029/2009GL040502.
Pagli, C., H. Wang, T. J. Wright, E. Calais, and E. Lewi (2014), Current plate boundary deformation of the afar rift from a 3-D velocity field inversion of InSAR and GPS, *J. Geophys. Res. Solid Earth*, *119*, 8562–8575, doi:10.1002/2014JB011391.
Pedersen, R., F. Sigmundsson, and T. Masterlark (2009), Rheologic controls on inter-rifting deformation of the northern volcanic zone, Iceland, *Earth Planet. Sci. Lett.*, *281*(1), 14–26.
Peltier, A., V. Ferrazzini, T. Staudacher, and P. Bachèlery (2005), Imaging the dynamics of dyke propagation prior to the 2000–2003 flank eruptions at Piton de la fournaise, reunion island, *Geophys. Res. Lett.*, *32*, L22302, doi:10.1029/2005GL023720.
Rivalta, E. (2010), Evidence that coupling to magma chambers controls the volume history and velocity of laterally propagating intrusions, *J. Geophys. Res.*, *115*, B07203, doi:10.1029/2009JB006922.
Rubin, A. M. (1992), Dike-induced faulting and graben subsidence in volcanic rift zones, *J. Geophys. Res.*, *97*(B2), 1839–1858.
Rubin, A. M., and D. Gillard (1998), Dike-induced earthquakes: Theoretical considerations, *J. Geophys. Res.*, *103*(B5), 10,017–10,030.
Rubin, A. M., and D. D. Pollard (1988), Dike-induced faulting in rift zones of Iceland and Afar, *Geology*, *16*(5), 413–417.
Ruegg, J.-C., and M. Kasser (1987), Deformation across the Asal-Ghoubbet rift, Djibouti, uplift and crustal extension 1979–1986, *Geophys. Res. Lett.*, *14*(7), 745–748.
Ruegg, J.-C., J.-C. Lepine, A. Tarantola, and M. Kasser (1979), Geodetic measurements of rifting associated with a seismo-volcanic crisis in Afar, *Geophys. Res. Lett.*, *6*(11), 817–820.
Ruegg, J.-C., M. Kasser, and J.-C. Lépine (1984), Strain accumulation across the Asal-Ghoubbet rift, Djibouti, East Africa, *J. Geophys. Res.*, *89*(B7), 6237–6246.
Savage, J. (1983), A dislocation model of strain accumulation and release at a subduction zone, *J. Geophys. Res.*, *88*(B6), 4984–4996.
Sigmundsson, F., et al. (2014), Segmented lateral dyke growth in a rifting event at Bardarbunga volcanic system, Iceland, *Nature*, *517*, 191–195.
Souriau, A., A. Cazenave, R. B. G. Balmino, K. Domlnh, P. Mazzega, J.-M. Lemolne, J.-C. Ruegg, C. Boucher, P. Wllls, and M. Kasser (1991), Present-day plate motions: Retrieval from The TOPEX/POSEIDON Orbitography Network (DORIS System), In JPL, TOPEX/Poseidon Science Investigations Plan (SEE N93-14964 04-48), 131–136.
Speight, J., R. Skelhorn, T. Sloan, and R. Knaap (1982), The dyke swarms of Scotland, in *Igneous Rocks of the British Isles*, edited by D. S. Sutherland, pp. 449–59, Wiley, Chichester, England.
Stein, R. S., P. Briole, J.-C. Ruegg, P. Tapponnier, and F. Gasse (1991), Contemporary, Holocene, and Quaternary deformation of the Asal Rift, Djibouti: Implications for the mechanics of slow spreading ridges, *J. Geophys. Res.*, *96*(B13), 21,789–21,806.
Tarantola, A., and B. Valette (1982), Generalized nonlinear inverse problems solved using the least squares criterion, *Rev. Geophys. Space Phys.*, *20*(2), 219–232.
Tarantola, A., J.-C. Ruegg, and J.-C. Lépine (1979), Geodetic evidence for rifting in Afar a brittle-elastic model of the behaviour of the lithosphere, *Earth Planet. Sci. Lett.*, *45*(2), 435–444.
Tarantola, A., J.-C. Ruegg, and J.-C. Lepine (1980), Geodetic evidence for rifting in Afar, 2. Vertical displacements, *Earth Planet. Sci. Lett.*, *48*(2), 363–370.
Tazieff, H., and J. Varet (1972), Tectonic significance of the Afar (or Danakil) depression, *Nature*, *235*, 144–147.
Tizzani, P., M. Battaglia, G. Zeni, S. Atzori, P. Berardino, and R. Lanari (2009), Uplift and magma intrusion at Long Valley caldera from InSAR and gravity measurements, *Geology*, *37*(1), 63–66.
Vigny, C., P. Huchon, J.-C. Ruegg, K. Khanbari, and L. M. Asfaw (2006), Confirmation of Arabia plate slow motion by new GPS data in Yemen, *J. Geophys. Res.*, *111*, B02402, doi:10.1029/2004JB003229.
Vigny, C., J.-B. de Chabalier, J.-C. Ruegg, P. Huchon, K. L. Feigl, R. Cattin, L. Asfaw, and K. Kanbari (2007), Twenty-five years of geodetic measurements along the Tadjoura-Asal rift system, Djibouti, East Africa, *J. Geophys. Res.*, *112*, B06410, doi:10.1029/2004JB003230.
Wright, T. J., C. Ebinger, J. Biggs, A. Ayele, G. Yirgu, D. Keir, and A. Stork (2006), Magma-maintained rift segmentation at continental rupture in the 2005 Afar dyking episode, *Nature*, *442*(7100), 291–294.